localization of the boron compound has not been performed. To overcome this weakness of BSH, several drug delivery systems (DDS) have been reported using therapeutically useful doses of BSH-containing pharmacophores [9]. Protein transduction therapy with cell-membrane penetrating peptides (CPPs) and a protein/peptide transduction domain (PTD) has marked advantages to get several materials (e.g. protein, peptide, small-interfering RNA) into cells without toxicity *in vitro* and *in vivo* [10–15]. Well-known intracellular transduction domain peptides, including the HIV trans-activator of transduction (TAT; aa 48–60 or 47–57), poly-arginine domain (11R and R9), antennapedia (Antp; aa 43–58) etc; have been reported as CPPs and PTD [16]. The mechanism of intracellular delivery using these peptide domains is proposed as a three-step process: first, binding of the CPPs to the cellular membrane with electrical interaction between CPPs and the cell membrane; second, stimulation of intracellular uptake by macropinocytosis; and third, release from macropinosomes into the cytoplasm [17].

In this time, we will try to prove that the intracellular localization of the boron compound is a marked advantage in BNCT and CPPs could be applied as a delivery system to carry a boron compound (BSH) into malignant glioma cells *in vitro* and *in vivo* for BNCT.

2. Materials and methods

2.1. Simulations of energy deposition in the nucleus for the local distribution of ^{10}B in one cell

There have been some previous works on the estimation of energy deposition at the cell level for BNCT [18–20]. Referring to these previous works, the influence of energy deposition in the cell nucleus for the local distribution of ^{10}B in a cell was assessed using analytical and stochastic methods. Fig. 1-A shows the geometry and mathematical expression for this assessment. The shapes of the cell and cell nucleus were supposed to be spherical. The contributions from ^{10}B distributed outside and inside of the nucleus were assessed separately. For the contribution from outside ^{10}B, the probabilities of the alpha particle and ^{7}Li nucleus generated due to $^{10}B(n,\alpha)^{7}Li$ were calculated geometrically for the incidence in the nucleus at a certain angle. The particle energy, for entering and exiting the cell nucleus, was calculated for each angle, considering the stopping powers [21,22]. The difference of these particle energies was regarded as the deposited energy in the cell nucleus.

For the contribution from inside ^{10}B, the probabilities of the generated particles for going forward in a certain direction were calculated geometrically. The energy lost until the particle exited the cell nucleus was calculated considering the stopping power. This lost energy was regarded as the deposited energy in the cell nucleus.

Integrating the above-calculated energy depositions into the weight of the angle and the ^{10}B distribution, the average energy deposition in the cell nucleus due to a $^{10}B(n,\alpha)^{7}Li$ reaction was estimated. Here, assessments were performed for five conditions of ^{10}B distribution; ① uniformly distributed in the whole cell, ② locally distributed only in the cell membrane, ③ uniformly distributed in cytoplasm, ④ locally distributed only in the nuclear membrane, and ⑤ uniformly distributed in the cell nucleus. The radius of the cell was fixed at 5 μm, and the radius of the cell nucleus was varied among 2, 2.5 and 3 μm.

2.2. Glioma cell lines

U87 DEGFR and PA U87 glioma cell lines (kindly donated by Professor Cavenee and Dr. Mukasa of the University of California at San Diego) were used in all experiments. U87 DEGFR cells stably express constitutively active EGFR, EGFRvIII, whereas PAU 87 cells not overexpress EGFR. The cells were maintained in Dulbecco's modified Eagle's medium (DMEM) (Invitrogen) with 10% fetal bovine serum (FBS), penicillin and streptomycin at 37 °C in a humidified atmosphere containing 5% CO_2.

2.3. Cell proliferation assay (WST-1 assay)

Cell Viability Assay—Cell viability was determined using a WST-1 assay (Roche Applied Science) as described previously [11]. After glioma cells (1×10^3/well) were seeded in 96-well flat-bottomed plates, they were cultured in Dulbecco's modified Eagle's medium containing 10% FBS for 24 h. The cells were then supplemented with various concentrations of BSH or BSH-peptide and further incubated for 24 h (day 1), 48 h (day 2), 72 h (day 3) and 96 h (day 4). Cell viability was measured using the WST-1 assay each day according to the manufacturer's instructions (Roche Applied Science).

2.4. Immunohistochemical analysis (IHC) and measurement of ^{10}B content in vitro

IHC was carried out to analyze the distribution of BSH *in vitro*. Cells were incubated for 1 h, 3 h, 6 h and 24 h with BSH and BSH-peptide. After incubation of boron compounds, the cells were thoroughly washed with PBS twice, fixed with 4% paraformaldehyde (PFA) for 10 min, and then incubated with anti-BSH mouse mAb [24]. The secondary antibody was Cy3 or Cy5-conjugated mouse IgG. Fluorescence signals were observed using a confocal laser microscope (FluoView; Olympus, Japan). To detect ^{10}B in cells, BSH or BSH-peptides were added to 6-cm dishes. After 2 h, 8 h and 24 h of incubation, the cells were washed with PBS, dissolved in 200 μL concentrated nitric acid overnight, and diluted with 5 mL MillQ water. The ^{10}B content was measured by inductively coupled plasma-atomic emission spectrometry (ICP-AES, Vista Pro, Seiko Instruments; Japan) as described previously [23,24].

2.5. Brain tumor model and detection of BSH-peptide in vivo

U87 ΔEGFR cells (3×10^5 cells/5 μL) were injected into the striatum of female 4–6 week-old nude mice (15–20 g, BALB/c Slc-nu/nu; Japan SLC) as described [24]. After two weeks, boron 0.7 mg-boron/200 μL of 8BSH-peptide or BSH was administered into tumor-bearing mice intravenously via the tail. After 6 h and 24 h, the mice were sacrificed and the brains were placed in PBS. Sections of 10-μm thickness were cut on a microtome (CM 1850; Leica Microsystems, Wetzlar, Germany). IHC was carried out as described previously and observed with a confocal laser microscopy [23,24].

2.6. Multi BSH-peptide synthesis

BSH was purchased from Katchem (Prague, Czech Republic) and all BSH-peptides were synthesized at KNC Laboratories Co. Ltd (Kobe, Japan).

2.6.1. $[Cys(Npys)]_8$-$(Lys)_7$-Arg-Arg-Arg-Arg-Arg-Arg-Arg-Arg-Arg-Arg-Arg-Arg-NH_2

The desired fully protected peptides resin was assembled using an Applied Biosystems model 433 peptide synthesizer with Fmoc-NH-SAL-PEG resin (0.18 mmol/g、0.25 mmol) as the starting solid support, as shown in Fig 3. Fmoc-Arg(Pbf), Fmoc-Lys(Fmoc), Boc-Cys(Npys) were used as amino acid materials The obtained $[Boc\text{-}Cys(Npys)]_8\text{-}(Lys)_7\text{-}Arg(Pbf)_{11}\text{-}NH\text{-}SAL\text{-}PEG$ resin was treated with the usual deprotecting reagents (TFA-TIS-H_2O (95/2.5/2.5/v/v)) at room temperature for 2 h. The desired crude S-Npys title peptide derivatives were isolated and purified by RP-HPLC.

2.6.2. $[Cys(BSH)]_8$-$(Lys)_7$-Arg-Arg-Arg-Arg-Arg-Arg-Arg-Arg-Arg-Arg-Arg-Arg-NH_2

To a solution of S-Npys peptide (35 mg 7.46 μmol) in water-CH3CN-DMSO (6/1/3 ml) was added solid $B_{12}SH\cdot$ 2Na (11.6 mg, 54.9 μmol) and stirred at room temperature for 6 h. The reaction mixture was then directly applied to the following preparative HPLC purification procedure. The purified titled BSH peptide was obtained as 13.4 mg (37.6% yield) as the lyophilized TFA salt products.

RP-HPLC Purity: 98.7%, MW:4771.95 (C132H355B96N67O26S10),m/z 1592.4 ($[M+3H]^{3+}$ 1591.7), m/z 328.7 ($[M+TFA+15H]^{15+}$ 326.7), m/z279.4 ($[M+17H]^{17+}$ 281.7)

Cys(BSH)-Arg11-NH_2

Cys(BSH)-Arg-Arg-Arg-Arg-Arg-Arg-Arg-Arg-Arg-Arg-Arg-NH_2, MW:2001.37, C69H152B12N46I2S2, MS : m/z 668.4 ([M+3H]3+668.13, m/z 706.5 ([M+TFA+3H]3+706.14 m/z 782.3 ([M+3TFA+3H]3+782.16

Cys(BSH)-Lys[Cys(BSH)-]Arg11-NH_2

Cys(BSH)-Lys[Cys(BSH)-]-Arg-Arg-Arg-Arg-Arg-Arg-Arg-Arg-Arg-Arg-Arg-NH_2

MW : 2394.1 C78H177B24 N49O14 S4, MS : m/z398.9 (M+12H.)12+ 398.7

[Cys(BSH)]4-(Lys)3-Arg11-NH_2

[Cys(BSH)]8-(Lys)7-Arg-Arg-Arg-Arg-Arg-Arg-Arg-Arg- Arg-Arg-Arg-NH_2

MW : 3181.4 C98H231B48N55O18 S8, MS : m/z 399.4 ([M+8H]8+ 398.7, m/z376.2 (M+5TFA+10H.)10+ 376.1

2.7. Cell proliferation assay with neutron radiation in research reactor

U87 delta EGFR cells were incubated with 0.1, 1, or 10 μM 8BSH-11R or 0.8, 8, 80, 800, or 8000 μM BSH for 6 h at 37 °C and 5% CO_2 in an incubator. After the incubation of boron compounds, glioma cells were washed with PBS twice and then irradiated with neutrons in Kyoto University research reactor (KUR) for 30 min (1 MW, rate of thermal neutron fluence 2.9–3.7 $\times$ $10^{12}/cm^2$, rate of epithermal neutron fluence 5.2–6.5 $\times$ $10^{11}/cm^2$). After irradiation, to check the early-stage BNCT reaction, the cells were separated into 3000 cells per well in a 96-well plate (each group $n = 6$) with culture medium and the WST-1 assay was performed 24 h and 48 h after neutron irradiation. To evaluate the late-stage BNCT effect, 5000 cells per 35 mm dish (each group $n = 6$) were cultured for 2 weeks and evaluated by colony formation assay with methanol fixation and 2% Giemsa solution staining [25].

2.8. Statistical analysis

Data are shown as the mean ± S.D. Data were analyzed using Student's *t*-test to compare the two conditions, and $p < 0.05$ was considered significant.

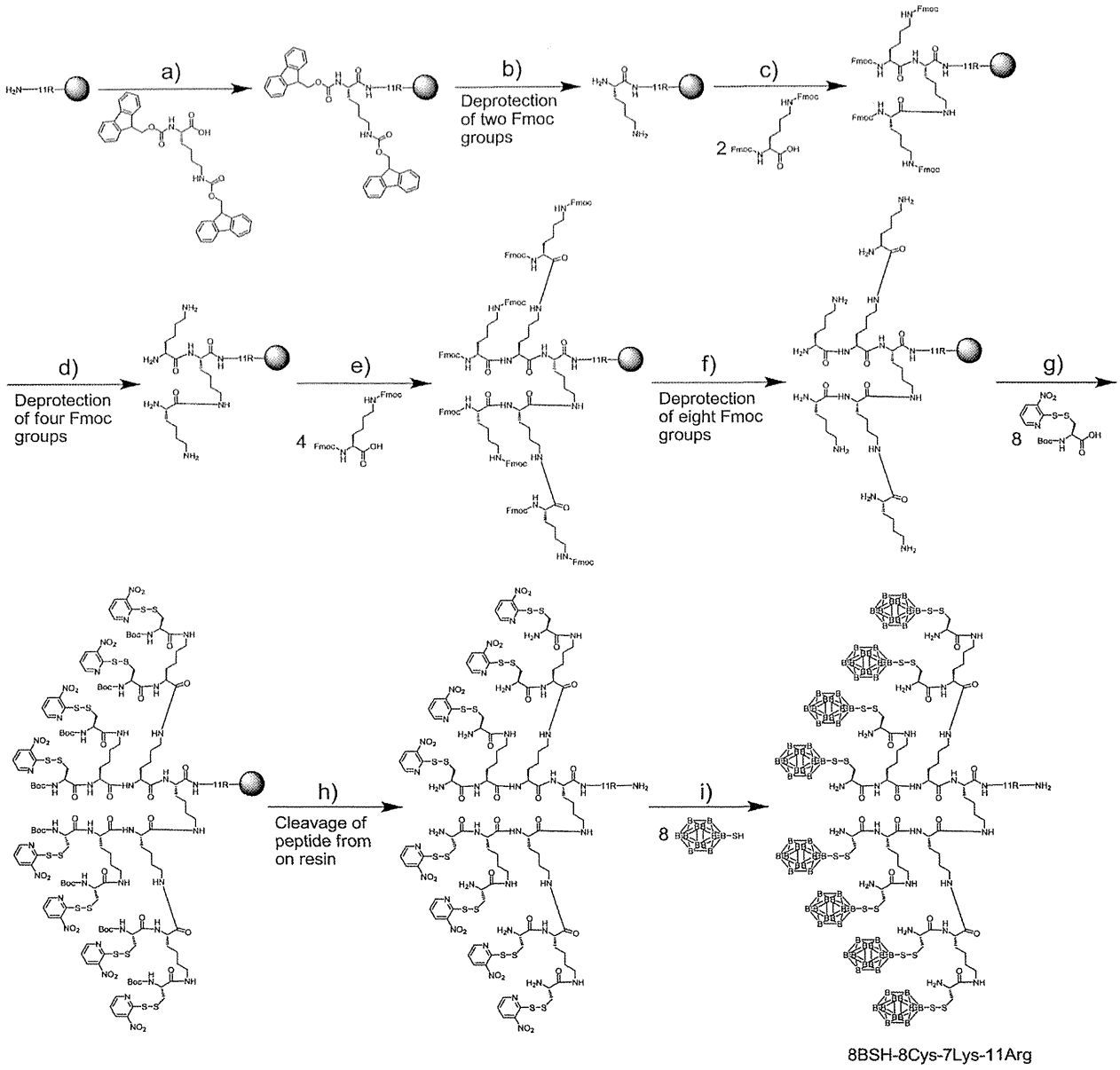

Fig. 2. Synthetic route of 8BSH-8Cys-7Lys-11Arg. Starting material is resin containing amino groups on the surface. a),c),e) Fmoc-Lys(Fmoc)(2eq), coupling reagents: HBTU, HOBt(2eq each),DIEA(4eq)/NMP; b),d),f) 20% piperidine/NMP; g) Boc-Cys(Npys)(4eq), coupling reagent DIC(4eq)/NMP; h) Trifluoroacetic acid/water/triisopropylsilane (=95/2.5/2.5 v/v/v); i) BSH.

3. Results

3.1. Simulations of changes in the energy deposition at one cell level for the radius of the cell nucleus

Suppl. Fig. 1 and Table 1 show the energy transfer ratio to the cell nucleus for the cell and nucleus radii. In Suppl. Fig. 2, the three curves correspond to three of the above-mentioned ^{10}B distributions, such as uniformly in the cell, cytoplasm only and nucleus only, forcell radii of 5, 7.5 and 10 μm. Under all distribution conditions, the average ^{10}B concentration in the whole cell was equal to 1 ppm. For any cell-nucleus radius, the energy deposition was normalized for local distribution only in the cytoplasmic membrane to 100%, because the boron compound of BSH cannot penetrate the cell membrane and we aimed to show the different effectiveness of an inside-cell or outside-cell boron compound with neutron irradiation.

It was found that the energy deposition markedly decreased when ^{10}B was not taken up into or near the cell nucleus, even for the same average ^{10}B concentration in the whole cell. As the cell nucleus is smaller, the effect of ^{10}B localization to the cell nucleus is larger. In the comparison of the absolute values, the energy deposition in the nucleus relatively increased as the cell nucleus became larger, for any condition of ^{10}B distribution. These three curves correspond to three of the above-mentioned ^{10}B distributions. Under any distribution condition, the average ^{10}B concentration in

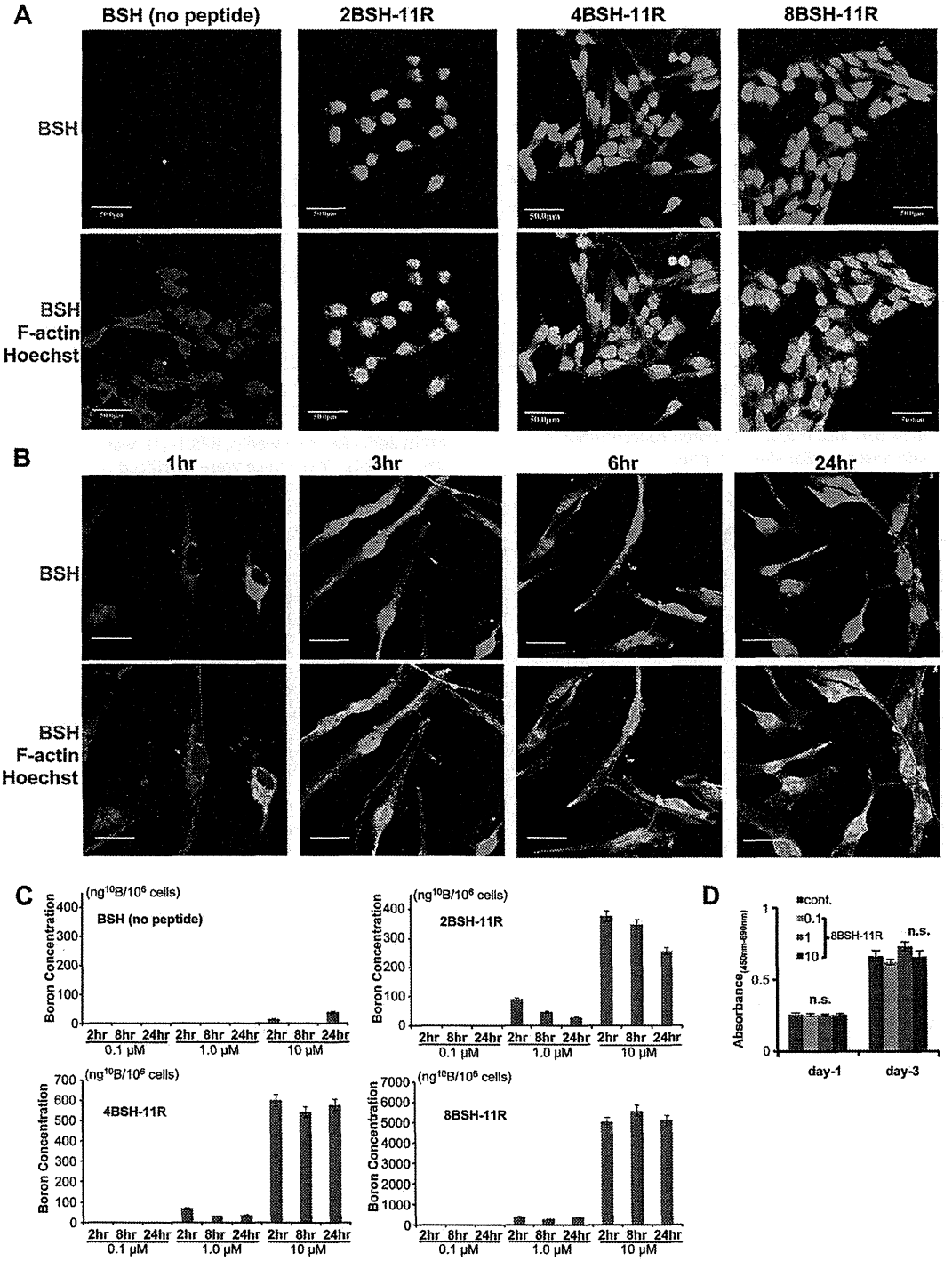

Fig. 3. BSH localization in glioma cells and boron ICP results of multi-BSH-11R (2BSH, 4BSH and 8BSH) 3-A: Confocal imaging of U87 delta EGFR cells showing BSH localization (green), cytoplasm (f-actin, red) and nucleus (Hoechst, blue) with 10 μM BSH, 2BSH-11R, 4BSH-11R and 8BSH-11R intracellular BSH localization in U87 delta EGFR cells for 12 h. Scale bar = 50 μm. 3-B: Immunocytochemistry showing BSH (green), f-actin (red), nucleus (blue) 1, 3, 6, and 24 h after administration of 10 μM 8BSH-11R. 3-C: ICP results showing B10 concentration in U87 delta EGFR cells with 0.1, 1, 10 μM BSH or BSH-peptide 2, 8, and 24 h after administration for ngB^{10} per 10^6 cells. 3-D: Cell proliferation results of U87 delta EGFR cells with control, 0.1, 1.0 and 10 μM 8BSH-11R for 1 or 3 days measured with WST-1 for absorbance (450 nm-690 nm). (For interpretation of the references to colour in this figure legend, the reader is referred to the web version of this article.)

Table 1
Calculated value of the local energy transfer ratio against nucleus % cytoplasm-membrane control from Fig. 1.

Cell radius (μm)	Nucleus radius (μm)	Energy transfer ratio to nucleus (% cytoplasm-membrane control)				
		Nucleus only	Nuclear-membrane only	Cytoplasm only	Cytoplasm-membrane only	Uniformly distributed
5	2.5	3370	900	317	100	592
7.5	2.5	13,100	3490	371	100	827
7.5	5	2090	570	206	100	746
10	2.5	104,000	27,700	1420	100	2990
10	5	9320	2540	458	100	1540
10	7.5	1940	507	205	100	917

the whole cell was equal to 1 ppm. For any cell-nucleus radius, the energy deposition was normalized to the uniform distribution in the whole cell to 100%.

In particular, Table 1 shows that the energy transfer ratio to the nucleus in nucleus-only localization was almost 30–1000 times different form cytoplasm membrane localization. Boron localization in the cytoplasm membrane control led the outside cell localization and outside cell-to-cell space in an *in vivo* model.

3.2. Intracellular BSH localization and boron concentration of glioma cells administrated BSH-fused peptide

BSH-peptide was produced with S–S connection between peptidesCys-NPYS and SH of BSH. The administration of BSH-fused CPPs (TAT:GRKKRRQRRR and 11R:RRRRRRRRRRR) to glioma cells showed high boron concentration according to the amount of administrated BSH-CPPs (Fig. 1-A), and BSH was clearly observed in U87 delta EGFR cells in the cytoplasmic region but not in the nuclear area (Fig. 1-B). On the other hand, BSH and BSH-NLS (NLS: PKKKRKV) administrated glioma cells did not demonstrate BSH inside the cell on immunohistochemistry with BSH antibody. The intracellularly transduced BSH was not toxic to glioma cells in the WST-1 assay for 4 days (Fig. 1-C).

3.3. Synthesis of 8BSH-8Cys-7Lys-11Arg (8BSH-11R)

The 8BSH-8Cys-7Lys-11Arg (8BSH-11R) was synthesized by disulfide linkage between the Cys(Npys)-activated cell-penetrating peptide (CPP) containing a peptide dendrimer and the BSHs after the CPP was prepared by Fmoc-based solid-phase peptide synthesis (SPPS) [26]. The sequence of peptide moiety is N′-Lys(Lys(Lys(H-Cys(Npys)2)2)2)-Arg11-NH_2-C′; Npys = 3-nitro-2-pyridinesulfenyl group. The synthesis route of 8BSH-11R is shown in Fig. 2. The structure contains multiple boron clusters and one CPP, and such a dendritic structure containing one CPP has seldom been reported [27].

3.4. Transduction of multi-BSH fused CPP into malignant glioma cells

BSH-11R could enter glioma cells, but was localized in the cytoplasm. BSH-11R's boron content ratio was only a few percentage of total molecular weight. To improve the boron content in one BSH-peptide, multi-BSH-fused CPPs (2BSH, 4BSH, and 8BSH) were synthesized. After administration, all multi-BSH fused 11R could enter cells and almost all was localized in the nucleus (Fig. 3-A). The time course imaging of 8BSH-11R-administrated glioma shows the change from cytoplasmic localization (1 h) to whole cell existence (3 h and 6 h) (Fig. 3-B). In particular 24 h after administration, almost all BSH was localized in the nucleus. Malignant glioma cells administrated with each multi-BSH-11R (2BSH-11R, 4BSH-11R, 8BSH-11R) showed a high concentration of intracellular boron concentration in direct proportion to the number of connected BSH in ICP results (Fig. 3-C, Table 2). In the 10 μM 8BSH-11R group, the boron content amount was almost 5000 ppm in 10^6 cells. Despite using a high-concentration BSH-peptide, this was no toxicity to the cells (Fig. 3-D).

3.5. In vivo 8BSH-11R distribution in intracranial brain tumor model

U87 delta EGFR glioma cells were implanted into a nude mouse brain and, after two weeks, 8BSH-11R was injected through the tail vein [23,24]. These mice were sacrificed 6 h and 24 h after the injection. Human GFAP antibody specifically stained only human GFAP that showed U87 delta EGFR cells. In low magnification results, 8BSH-11R was localized in the tumor and peripheral tumor area (Fig. 4-A). Almost all 8BSH-11R was co-localized with human glioma cells at 6 h and 24 h. In high magnification observation, 8BSH-11R had definitely transduced into the tumor center and tumor edge, but not into the normal brain at 6 h and 24 h (Fig. 4-B, C). 8BSH-11R in the tumor area and at the tumor edge could enter cells and was localized in the nucleus and cytoplasm. On the other hand, 8BSH-11R could not be detected in the normal brain area on high magnification confocal microscopy (Fig. 4-B, C).

3.6. BNCT effect after neutron irradiation with BSH or 8BSH-11R against malignant glioma

8BSH-11R or BSH was administrated to glioma cells at the point of equalization of boron content. With neutron radiation for 30 min, 1 kW (thermal neutron fluence $3.2 \times 101^2/cm^2$) at Kyoto University Reactor Institute, after neutron irradiation, early-stage (24 h and 48 h after neutron radiation) and late-stage (2 weeks after neutron radiation) BNCT effects were evaluated separately with the WST-1 assay and colony formation assay. As early effects on cell proliferation, the 1 μM- and 10 μM- administrated 8BSH-11R groups showed marked cell growth inhibition at both 24 h and 48 h compared to the 100 or 1000 times more BSH-administrated group (Fig. 5-A). Furthermore, in the colony formation assay 2 weeks after BNCT, 8BSH-11R 1 μM and 10 μM groups had no colony formation. 800 μM and 8 mM BSH groups showed slight cell growth inhibition effects compared to the control group (Fig. 5-B, C).

Table 2
B^{10} ICP-AES results in U87 delta EGFR cell from Fig. 4-C.

^{10}B ICP-AES data *in vitro*		
Name of boron compound	^{10}B con. ($ng^{10}B/10^6$ cells) 10 μM to U87 ΔEGFR	Boron ratio (%)
BSH	15.9[a]	57.4
BSH-11R	219.4	6.0
2BSH-11R	391.4	10.0
4BSH-11R	588.8	15.1
8BSH-11R	5623.7	20.1

[a] BSH without CPPs could not penetrate cell membrane.

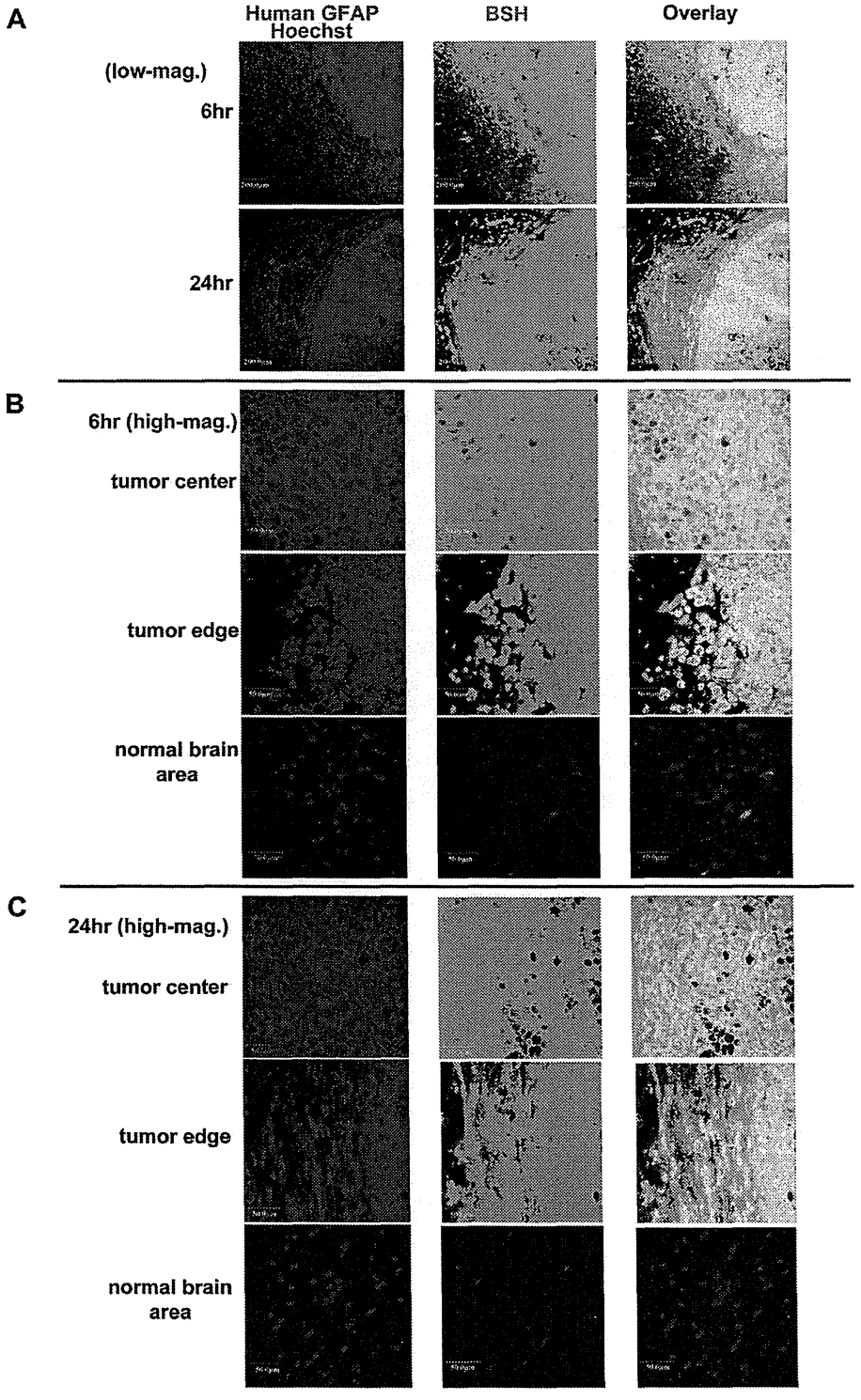

Fig. 4. Confocal imaging showing immunohistochemistry of BSH in mouse brain tumor model with injection into mouse tail vain 4-A: Confocal imaging of brain tumor slices at low magnification showing human-specific detected GFAP (brain tumor area: red), BSH (green), nucleus (blue) 6 or 24 h after mouse tail vein injection of 8BSH-11R. Scale bar = 200 μm 4-B, C: Immunohistochemistry imaging of the tumor core area (tumor center), tumor border zone (tumor edge) and normal brain area (normal brain) showing human GFAP (red), BSH (green) and nucleus (blue), Scale bar = 50 μm. (For interpretation of the references to colour in this figure legend, the reader is referred to the web version of this article.)

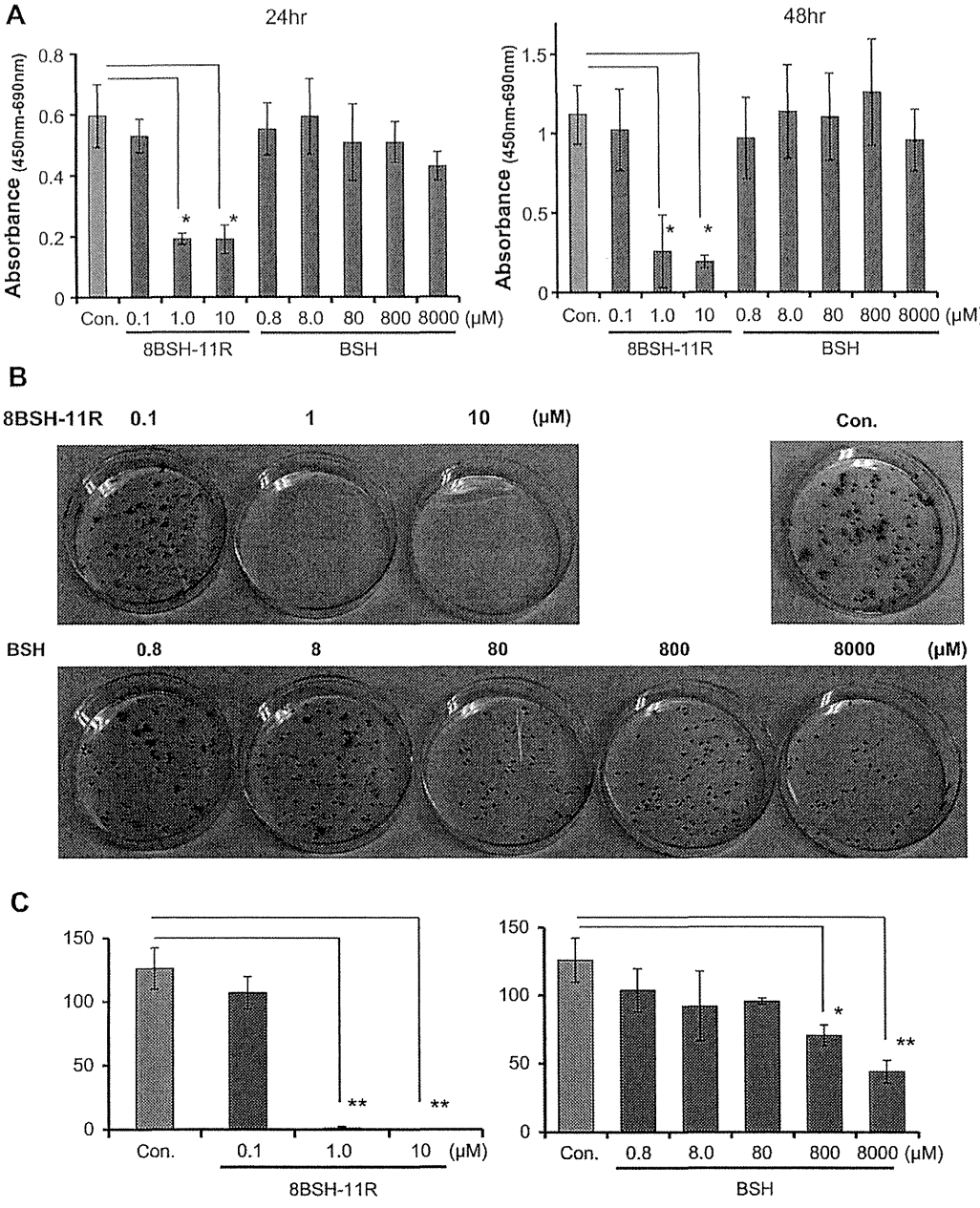

Fig. 5. Cell proliferation results with administration of BSH or 8BSH-11R after neutron irradiation by nuclear reactor 5-A: WST-1 assay showing early-stage damage of BNCT to malignant glioma cells (U87 delta EGFR) 24 and 48 h after neutron irradiation at each different BSH or 8BSH-11R concentration. All data were measured at the absorbance 450 nm-690 nm. *$p < 0.01$ 5-B, C: Colony formation assay results showing late-stage damage of BNCT to glioblastoma cells with different doses of BSH or 8BSH-11R. *$p < 0.05$, **$p < 0.01$.

4. Discussion

The nuclear reaction effectiveness of BNCT is a very limited area with alpha decay that induces alpha particles and lithium-7 nuclei and induces specific cell death through the double strand break of DNA [3,25]. BNCT is not only next-generation therapy but also one of the most anticipated treatments in the short-term against various malignant refractory tumors [28]. One of the most difficult problems in BNCT to develop the next stage for clinical use is to develop new and useful boron compounds beyond the present boron agent, BSH. A clinical trial with high-dose BPA (900 mg/kg) in BNCT against glioblastoma patients in Sweden showed no survival improvement compared to standard therapy [29]. However, the combination use of BPA (700 mg/kg) and BSH (100 mg/kg) in BNCT against glioblastoma patients with additional X-ray irradiation therapy induced a very good outcome by the Osaka Medical University group, Japan [2]. The combined use of BSH and BPA is the key to BNCT success in glioblastoma therapy. BPA can pass through the blood brain barrier (BBB) and accumulate in the tumor [5]. BPA is taken up into cells through L-type amino acid transporter 1 (LAT-

1), which can transport neutral amino acids with a relatively bulky aromatic side chain (e.g. phenylalanine and tyrosine) [30–32] LAT-1 highly expresses many malignant tumor cell lines including glioma cells and a few normal organs (e.g. brain and placenta). On the other hand, BSH is an anionic boron cluster, but cannot enter cells by itself. Regarding the anti-cancer effect of BNCT, extracellular boron localization in cancer cells is less effective than intracellular boron; however, there is no clear evidence or simulations about the relationship between boron localization and nuclear energy transfer on a cellular level. In our simulation results, the cell membrane localization of 1ppm boron showed only 1/30–1/1000 times energy deposition in the nucleus with neuron irradiation. This showed a very clear direction to innovate a new boron compound from BSH. We consider that the combined use of BSH and BPA is essential for glioblastoma treatment from Japanese BNCT clinical data and the next plan to improve the survival outcome will depend on the improvement of BSH. Several reports about boron delivery systems (BDS) have shown the good effectiveness to develop intra-cellular transducible BSH, but this peptide BDS is reported for the original in BNCT research [23,24,33–36]. BSH, CPPs and BSH-CPPs were not toxic and were very safe in clinical use [11,37]. The 8BSH-11R-administrated group with neutron irradiation showed a very strong tumor killing effect compared to the BSH-administrated group. Regarding effectiveness in the brain tumor model, 8BSH-11R localized specifically in the tumor area and inside malignant glioma cells and long-term accumulation in the tumor was maintained (Fig. 4). Interestingly, 8BSH-11R did not show uptake into the normal brain area for enhanced permeability and retention (EPR) effects.

Delivering multiple boron clusters into cells by CPP is economical, safe and effective in respect of medical treatment because one CPP can carry many BSHs while maintaining a high of boron ratio of one boron molecule in the cell; that is using, the peptide dendrimer it is expected that the cell will be destroyed by concentrated boron clusters with a sufficient effect of BNCT, when a small amount of the peptide dendrimer is carried into cells. Since a well-defined peptide dendrimer can be prepared with simple SPPS and organic synthesis, this peptide dendrimer is expected to be used in the application of medical treatment that differs from the drug delivery of dendrimers reported by other groups [38–43].

This is the original paper on a new boron compound with a peptide delivery system *in vitro* and *in vivo*. Some papers have pointed out the toxicity of BDS with liposomes, whereas, the peptide delivery system with CPPs is very safe and is anticipated to be used for clinical applications. In this study, we used 11R, the polyarginine domain and TAT as CPP for BDS, aiming for clinical application in BNCT [36]. Several reports have pointed out that DDS with CPP transduction therapy needs repeated administration to maintain a continuous long-term effect *in vivo* in cancer treatment [44]. Considering that BNCT is usually only once treatment, this application of BDS is ideal for the development of CPP therapy [45]. Our results showed that the malignant glioma cells in the 8BSH-11R group had inhibited tumor growth with a very low concentration of BSH-peptide administration compared to the clinical use of BSH with neutron radiation. The ingenious use of BSH in BNCT, such as its combination with CPPs, offers a new direction for new BDS (Table 3). Recently, many functional peptides have been reported for tumor targeting, low-pH sensitive peptide (pH Low Insertion Peptide: pHLIP), hypoxia region stable domain (oxygen degradation domain: ODD) and many tumor surface receptor targeting peptides [46–48]. We can apply these peptides with important functions against various cancers to deliver boron peptide. Hence, this new boron compound with functional peptide use will contribute to enhancing safe and effective BNCT as a next-generation major cancer therapy.

Table 3
A chart of BSH-fused peptide plan from present BSH compound to next generation of BSH-peptides.

	BSH compound	Peptide vector	Advantages & disadvantages
Present BSH	BSH	No	No BBB passage, No uptake into cell High boron content
1st generation BSH-peptide	BSH-11R	11R (CPP)	Intracellular transduction with CPP Low boron content
2nd generation BSH-peptide	(BSH)n-11R	11R (CPP) Lys dendritic domain	Intracellular transduction High boron content No targeting function
3rd generation BSH-peptide	Target-peptide-(BSH)n-poly-Arg	Tumor-targeting domain Lys dendritic domain 11R or not	Intracellular transduction High boron content Targeting function

5. Conclusion

We made multi-linked mercaptoundecahydrododecaborate (BSH) fused cell-penetrating peptide, 11R and became successful for introducing safely into malignant glioma *in vitro* and *in vivo*. Intracellular boron compounds fused CPP showed strong tumor growth inhibition with neutron irradiation and.

BSH-peptide has potential to be the core boron agent in future boron neutron capture therapy.

Competing financial interests

The authors declare no competing financial interests.

Acknowledgments

We thank Prof. M Kirihata, Osaka Prefecture University, Japan, for the BSH monoclonal antibody for IHC *in vitro* and *in vivo*. We thank A. Ueda for technical assistance in our laboratory. This work was supported by a Grant-in-aid for Scientific Research from the Ministry of Education, Science, Sports, Culture of Japan, by a Grant-in-aid for Scientific Research from the Ministry of Health, Labor and Welfare of Japan, by a young researcher start-up grant from Okayama University, by Sekizenkai, a foundation of Okayama University Hospital. The authors gratefully thank Division of Instrumental Analysis, Department of Instrumental Analysis & Cryogenics, Advanced Science Research Center, Okayama University for the ICP measurements.

Appendix A. Supplementary data

Supplementary data related to this article can be found at http://dx.doi.org/10.1016/j.biomaterials.2013.12.055.

References

[1] Stupp R, Mason WP, van den Bent MJ, Weller M, Fisher B, Taphoorn MJ, et al. radiotherapy plus concomitant and adjuvant temozolomide for glioblastoma. N Engl J Med 2005;352(10):987–96.
[2] Kawabata S, Miyatake S, Kuroiwa T, Yokoyama K, Doi A, Iida K, et al. boron neutron capture therapy for newly diagnosed glioblastoma. J Radiat Res 2009;50(1):51–60.
[3] Locher GL. Biological effects and therapeutic possibilities of neutrons. Am J Roentgenol 1936;36:1–13.
[4] Soloway AH, Hatanaka H, Davis MA. penetration of brain and brain tumor. VII. tumor- binding sulfhydryl boron compounds. J Med Chem 1967;10:714–7.

[5] Miyatake S, Tamura Y, Kawabata S, Iida K, Kuroiwa T, Ono K. boron neutron capture therapy for malignant tumors related to meningiomas. Neurosurgery 2007;61(1):82–90.
[6] Barth RF. boron neutron capture therapy at the crossroads: challenges and opportunities. Appl Radiat Isot 2009;67(7–8 Suppl.):S3–6.
[7] Hatanaka H. a revised boron-neutron capture therapy for malignant brain tumors. J Neurol 1975;209:81–94.
[8] Imahori Y, Ueda S, Ohmori Y, Kuzuki T, Ono K, Fujii R, et al. fluorine-18-Labeled fluoroboronophenylalanine PET in patients with glioma. J Nucl Med 1998;39:325–33.
[9] Nakamura H, Miyajima Y, Takei T, Kasaoka S, Maruyama K. synthesis and vesicle formation of a nido-carborane cluster lipid for boron neutron capture therapy. Chem Commun 2004:1910–1.
[10] Matsushita M, Tomizawa K, Moriwaki A, Li ST, Terada H, Matsui H. a high-efficiency protein transduction system demonstrating the role of PKA in long-lasting long-term potentiation. J Neurosci 2001;21(16):6000–7.
[11] Michiue H, Tomizawa K, Wei FY, Matsushita M, Lu YF, Ichikawa T, et al. the NH_2 terminus of influenza virus hemagglutinin-2 subunit peptides enhances the antitumor potency of polyarginine-mediated p53 protein transduction. J Biol Chem 2005;280(9):8285–9.
[12] Michiue H, Tomizawa K, Matsushita M, Tamiya T, Lu YF, Ichikawa T, et al. ubiquitination-resistant p53 protein transduction therapy facilitates anti-cancer effect on the growth of human malignant glioma cells. FEBS Lett 2005;579(18):3965–9.
[13] Matsui H, Tomizawa K, Lu YF, Matsushita M. protein therapy: in vivo protein transduction by polyarginine (11R) PTD and subcellular targeting delivery. Curr Protein Pept Sci 2003;4(2):151–7.
[14] Nagahara H, Vocero-Akbani AM, Snyder EL, Ho A, Latham DG, Lissy NA, et al. transduction of full-length TAT fusion proteins into mammalian cells: TAT-p27Kip1 induces cell migration. Nat Med 1998;4(12):1449–52.
[15] Michiue H, Eguchi A, Scadeng M, Dowdy SF. induction of in vivo synthetic lethal RNAi responses to treat glioblastoma. Cancer Biol Ther 2009;8(23):2306–13.
[16] Gump JM, Dowdy SF. TAT transduction: the molecular mechanism and therapeutic prospects. Trends Mol Med 2007;13(10):443–8.
[17] Wadia JS, Stan RV, Dowdy SF. Transducible TAT-HA fusogenic peptide enhances escape of TAT-fusion proteins after lipid raft macropinocytosis. Nat Med 2004;10(3):310–5.
[18] Kobayashi T, Kanda K. analytical calculation of boron-10 dosage in cell nucleus for neutron capture therapy. Radiat Res 1982;91:77–94.
[19] Charlton DE, Allen BJ. Monte Carlo calculations of ion passages through brain endothelial nuclei during boron neutron capture therapy. Int J Radiat Biol 1993;64:739–47.
[20] Tung CJ, Liu CS, Wang JP, Chang SL. calculations of cellular microdosimetry parameters for alpha particles and electrons. Appl Radiat Isot 2004;61:739–43.
[21] Northcliffe LC, Schilling RR. range and stopping-power tables for heavy ions. Nucl Data Tab 1970;A7:233–463.
[22] ICRU Report 49 stopping powers and ranges for protons and alpha particles. Bethesda, MD, USA: International Commission on Radiation Units and Measurements; 1993.
[23] Feng B, Tomizawa K, Michiue H, Han XJ, Miyatake S, Matsui H. development of a bifunctional immunoliposome system for combined drug delivery and imaging in vivo. Biomaterials 2010;31(14):4139–45.
[24] Feng B, Tomizawa K, Michiue H, Miyatake S, Han XJ, Fujimura A, et al. delivery of sodium borocaptate to glioma cells using immunoliposome conjugated with anti-EGFR antibodies by ZZ-His. Biomaterials 2009;9:1746–55.
[25] Takahashi A, Matsumoto H, Nagayama K, Kitano M, Hirose S, Tanaka H, et al. evidence for the involvement of double-strand breaks in heat-induced cell killing. Cancer Res 2004;64(24):8839–45.
[26] Kitamatsu M, Kitabatake M, Noutoshi Y, Ohtsuki T. synthesis and properties of peptide dendrimers containing fluorescent and branched amino acids. Biopolymer 2013;100(1):64–70.
[27] Lim Y, Lee E, Lee M. controlled bioactive nanostructures from self-assembly of peptide building blocks. Angew Chem Int Ed 2007;46:9011–4.
[28] Barth RF, Coderre JA, Vicente MG, Blue TE. boron neutron capture therapy of cancer: current status and future prospects. Clin Cancer Res 2005;11:3987–4002.
[29] Henriksson R, Capala J, Michanek A, Lindahl SA, Salford LG, Franzén L, et al. boron neutron capture therapy (BNCT) for glioblastoma multiforme: a phase II study evaluating a prolonged high-dose of boronophenylalanine (BPA). Radiother Oncol 2008:183–91.
[30] Detta A, Cruickshank GS. L-amino acid transporter-1 and boronophenylalanine-based boron neutron capture therapy of human brain tumors. Cancer Res 2009;69(5):2126–32.
[31] Oda K, Hosoda N, Endo H, Saito K, Tsujihara K, Yamamura M, et al. L-type amino acid transporter 1 inhibitors inhibit tumor cell growth. Cancer Sci 2010;101(1):173–9.
[32] Kaira K, Oriuchi N, Otani Y, Shimizu K, Tanaka S, Imai H, et al. fluorine-18-alpha-methyltyrosine positron emission tomography for diagnosis and staging of lung cancer: a clinicopathologic study. Clin Cancer Res 2007;13(21):6369–78.
[33] Maruyama K, Ishida O, Kasaoka S, Takizawa T, Utoguchi N, Shinohara A, et al. intracellular targeting of sodium mercaptoundecahydrododecaborate (BSH) to solid tumors by transferrin-PEG liposomes, for boron neutron-capture therapy (BNCT). J Control Release 2004;98(2):195–207.
[34] Masunaga S, Kasaoka S, Maruyama K, Nigg D, Sakurai Y, Nagata K, et al. the potential of transferrin-pendant-type polyethyleneglycol liposomes encapsulating decahydrodecaborate-(10)B (GB-10) as (10)B-carriers for boron neutron capture therapy. Int J Radiat Oncol Biol Phys 2006;66(5):1515–22.
[35] Lee JD, Ueno M, Miyajima Y, Nakamura H. synthesis of boron cluster lipids: closo-dodecaborate as an alternative hydrophilic function of boronated liposomes for neutron capture therapy. Org Lett 2007;9(2):323–6.
[36] Nakamura H, Ueda N, Ban HS, Ueno M, Tachikawa S. design and synthesis of fluorescence-labeled closo-dodecaborate lipid: its liposome formation and in vivo imaging targeting of tumors for boron neutron capture therapy. Org Biomol Chem 2012;10(7):1374–80.
[37] Noguchi H, Matsushita M, Kobayashi N, Levy MF, Matsumoto S. recent advances in protein transduction technology. Cell Transplant 2010;19(6):649–54.
[38] Jansen JF, Debrabandervandenberg EM, Meijer EW. encapsulation of guest molecules into a dendritic box. Science 1994;266:1226–9.
[39] Esfand R, Tomalia DA. poly(amidoamine) (PAMAM) dendrimers: from biomimicry to drug delivery and biomedical applications. Drug Discov Today 2001;6:427–36.
[40] Higashi N, Koga T, Niwa M. enantioselective binding and stable encapsulation of alpha-amino aids in a helical poly(L-glutamic acid)-shelled dendrimer in aqueous solutions. ChemBioChem 2002;3:448–54.
[41] Inoue Y, Kurihara R, Tsuchida A, Hasegawa M, Nagashima T, Mori T, et al. efficient delivery of siRNA using dendritic poly(L-lysine) for loss-of-function analysis. J Control Release 2008;126:59–66.
[42] Haensler J, Szoka FC. polyamidoamine cascade polymers mediate efficient transfection of cells in culture. Bioconjug Chem 1993;4:372–9.
[43] Hardy JG, Kostiainen MA, Smith DK, Gabrielson NP, Pack DW. dendrons with spermine surface groups as potential building blocks for nonviral vectors in gene therapy. Bioconjug Chem 2006;17:172–8.
[44] van den Berg A, Dowdy SF. protein transduction domain delivery of therapeutic macromolecules. Curr Opin Biotechnol 2011;6:888–93.
[45] Snyder EL, Dowdy SF. recent advances in the use of protein transduction domains for the delivery of peptides, proteins and nucleic acids in vivo. Expert Opin Drug Deliv 2005;1:43–51.
[46] Aina OH, Liu R, Sutcliffe JL, Marik J, Pan CX, Lam KS. from combinatorial chemistry to cancer-targeting peptides. Mol Pharmacol 2007;4(5):631–51.
[47] Yao L, Danniels J, Moshnikova A, Kuznetsov S, Ahmed A, Engelman DM. pHLIP peptide targets nanogold particles to tumors. Proc Natl Acad Sci U S A 2013;110(2):465–70.
[48] Kaur B, Khwaja FW, Severson EA, Matheny SL, Brat DJ, Van Meir EG. hypoxia and the hypoxia-inducible-factor pathway in glioma growth and angiogenesis. Neuro Oncol 2005;2:134–53.

Futamura et al. Radiation Oncology 2014, 9:237
http://www.ro-journal.com/content/9/1/237

RADIATION ONCOLOGY

CASE REPORT Open Access

A case of radiation-induced osteosarcoma treated effectively by boron neutron capture therapy

Gen Futamura[1], Shinji Kawabata[1], Hiroyuki Siba[1], Toshihiko Kuroiwa[1], Minoru Suzuki[2], Natsuko Kondo[2], Koji Ono[2], Yoshinori Sakurai[3], Minoru Tanaka[4], Tomoki Todo[4] and Shin-Ichi Miyatake[5*]

Abstract

We treated a 54-year-old Japanese female with a recurrent radiation-induced osteosarcoma arising from left occipital skull, by reactor-based boron neutron capture therapy (BNCT). Her tumor grew rapidly with subcutaneous and epidural extension. She eventually could not walk because of cerebellar ataxia. The tumor was inoperable and radioresistant. BNCT showed a marked initial therapeutic effect: the subcutaneous/epidural tumor reduced without radiation damage of the scalp except hair loss and the patient could walk again only 3 weeks after BNCT. BNCT seems to be a safe and very effective modality in the management of radiation-induced osteosarcomas that are not eligible for operation and other treatment modalities.

Introduction

The incidence of radiation-induced sarcoma has been estimated to be between 0.03% and 0.3% of all patients who have received radiation therapy [1,2]. Radiation-induced osteosarcomas are being encountered more frequently as the use of radiation therapy becomes more common, and the number of long-term cancer survivors has increased. The original diagnostic criteria for radiation-induced osteosarcomas were proposed in 1948 by Cahan et al. [3], and a short latency period was recently accepted for these tumors [1,4,5]. The diagnosis of radiation-induced osteosarcoma must fulfill the following four criteria: (1) the sarcoma must arise in a previously irradiated field, (2) the sarcoma must be histologically distinct from the original neoplasm, (3) there was no evidence of tumor in the involved bone at the time of initial irradiation, and (4) there must be a latency period between the irradiation and the development of the sarcoma at least 3 years.

Radiation-induced osteosarcoma of the head is a devastating complication of radiation therapy. It is very rare but aggressive, with high recurrence and a poor prognosis [6]. The median overall survival time was reported to be 29 months [1]. Osteosarcoma is thought to be radioresistant [7,8]. Therefore, complete surgical resection has been described as the most important prognostic factor [9] and the first choice of treatment for radiation-induced osteosarcoma. However, if complete surgical resection is difficult (as it was in the present case), adjuvant chemotherapy and radiotherapy should be considered. These therapeutic effects have thus far been found to be insufficient, however. We report here the case of a patient with recurrent radiation-induced osteosarcoma who was treated effectively by boron neutron capture therapy (BNCT).

BNCT is based on the nuclear capture reactions that occur when non-radioactive boron-10 is irradiated with neutrons of the appropriate energy to yield high linear energy transfer (LET) alpha particles (4He) and recoiling lithium-7 (7Li) nuclei. Since these particles have short path-lengths of approximately one cell diameter, their lethality is primarily limited to boron-containing cells. Theoretically, high LET particles have the advantage to overcome radioresistance to photon radiotherapies (such as X-rays). BNCT can thus be regarded as tumor cell-selective and an intensive particle radiation modality with minimal damage to normal tissue, [10,11] even for X-ray-resistant tumors. Here we report a successfully treated a case of radiation-induced osteosarcoma by reactor-based BNCT.

Case report

A 54-year-old Japanese female was referred to our institute for treatment by BNCT of a recurrent radiation-induced

* Correspondence: neu070@poh.osaka-med.ac.jp
[5]Cancer Center, Osaka Medical College, Takatsuki, Japan
Full list of author information is available at the end of the article

osteosarcoma involving the left occipital bone. Ten years earlier, she was diagnosed with cancer of the uterine body and underwent resection surgery. Two years after that surgery, she underwent chemotherapy and whole-brain radiation therapy (WBRT, total 30 Gy with 10 fractions) including the cerebellum for brain metastasis. Six years after the WBRT, she was diagnosed with a radiation-induced osteosarcoma involving the left occipital bone, and she underwent resection surgery and successive chemotherapy using methotrexate. One year after that surgery and chemotherapy, the subcutaneous tumor appeared again in the left occipital region and rapidly enlarged over a period of only 3 months (Figure 1A). Magnetic resonance images (MRI) showed the epidural tumor invasion (Figure 2A and A'). Eventually, the patient could not walk because of acutely developing cerebellar ataxia. This tumor was diagnosed as a recurrence of the radiation-induced osteosarcoma in accord with the above Cahan's criteria [3].

We performed BNCT for the radiation-induced osteosarcoma because the lesion/normal brain (L/N) ratio of fluoride-labeled boronophenylalanine positron emission tomography (FBPA-PET) was enough high, as shown in Figure 3A and B (L/N ratio: 3.8) [12]. For the BNCT, neutron irradiation was applied at Kyoto University Reactor.

The patient was administered 500 mg/kg of BPA intravenously for 3.2 hours (200 mg/kg for initial 2 hours, prior to neutron irradiation, 100 mg/kg for 1.2 hours during neutron irradiation). The boron concentration in the blood was monitored by sampling every 1 hour after boron compound administration until neutron irradiation was completed. The boron concentrations from BPA in the tumor and normal brain were estimated from the L/N ratio of 18 F-BPA on PET. The neutron fluence rate was simulated by the dose-planning system, SERA (Idaho National Engineering and Environmental Laboratory, Idaho Falls, ID) and the total doses to the tumor and normal brain were simulated. The neutron irradiation time was determined not to exceed 13 Gy-Eq to the normal brain in accordance with our recent protocol of BNCT for high-grade meningiomas [10]. For this case, irradiation time was 70 minutes and B10 concentration of the venous blood was judged as 37.2 ppm during the neutron irradiation. Here, Gy-Eq (Gy: Gray) means an X-ray dose that can give biologically equivalent effects to total BNCT radiation. The scalp just above the tumor was covered with the bolus composed of sodium polyacrylate with 1 cm-thickness to gain the superficial neutron flux. After the treatment, the doses given were re-estimated precisely and are shown in Table 1. We hypothesized the boron concentrations of the blood, brain, and skin were equal, as we did in the previous BNCT. RBE and CBE values employed here were listed in Table 2.

Absorbed physical dose and X-ray-equivalent dose (Gy-Eq) are calculated with the following formula;

$$E_{Total} = E_{B10} + E_{Thermal} + E_{Fast} + E_{\gamma}$$

$$E_{B10} = (C_{BSH} \times CBE_{BSH} + C_{BPA} \times CBE_{BPA}) \times 7.43 \times 10^{-14} \times \Phi_{Thermal}$$

$$E_{Thermal} = N \times RBE_{Thermal} \times 6.78 \times 10^{-14} \times \Phi_{Thermal}$$

$$E_{Fast} = RBE_{Fast} \times D_{Fast}$$

$$E_{\gamma} = RBE_{\gamma} \times D_{\gamma}$$

D: physical absorbed dose (Gy),
ΦThermal: fluence of theraml neutron (cm-2),
N: nitrogen concentration (2%, here)
C: B10 concentration (ppm).

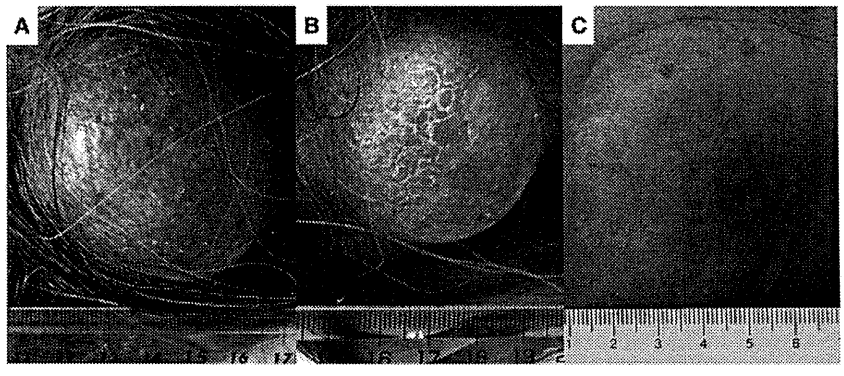

Figure 1 Marked improvement of the subcutaneous tumor at 3 weeks after the application of BNCT. A: Just prior to the BNCT; the tumor is elastic hard, and painful. **B**: Seven days after the BNCT; the tumor is soft and no longer painful. **C**: At 2 months after the BNCT, the tumor had shrunk drastically without radiation damage to the skin.

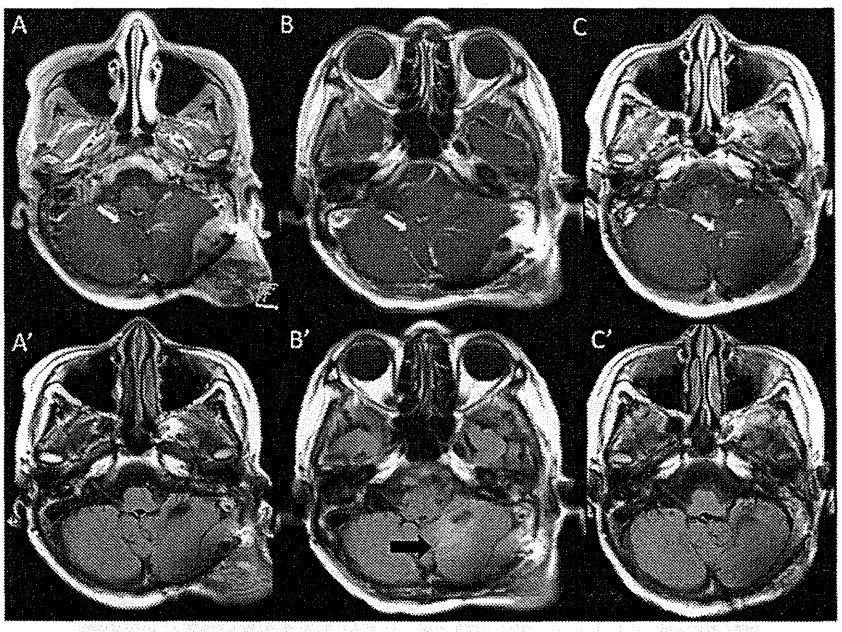

Figure 2 MRI of the patient's brain before and after the BNCT. White arrows indicate a venous angioma, which was recognized incidentally and judged as a sectional standard of MRI. **A**: Gd-enhanced T1-weighted MRI of the brain 1 month before the BNCT. There was a subcutaneous and epidural tumor mass. **B**: Gd-enhanced T1-weighted MRI at 4 days after BNCT. The tumor mass was reduced. **C**: Gd-enhanced T1-weighted MRI of the brain 3 months after BNCT. The tumor mass was further reduced. **A'**: Fluid-attenuated inversion recovery (FLAIR) MRI of the brain 1 month before BNCT. **B'**: FLAIR MRI of the brain 4 days after BNCT. The tumor mass was reduced, but the edema had worsened. A black arrow indicates the cerebellar edema. **C'**: FLAIR MRI of the brain 3 months after BNCT. The tumor mass was further reduced, and the edema had disappeared.

For this patient, we estimated that the minimum tumor and maximum normal brain and skin doses were 67.7, 12.7 and 12.4 Gy-Eq, respectively in the BNCT, simulated from F-BPA-PET imaging and the blood BPA concentration (Table 1).

At one day after the BNCT, the patient's gait disturbance was aggravated. Computed tomography at that time showed aggravation of peri-lesional edema (data not shown). Remarkably, the MRI taken 4 days after the BNCT demonstrated the definitive shrinkage of the mass, but the left cerebellar edema was still there (Figure 2B and B'). We then treated the edema with dehydrators and steroids. The symptoms gradually improved.

At only 3 weeks after the BNCT, the patient was able to walk again stably without aid. The subcutaneous tumor was reduced dramatically without radiation injury of the scalp, with time after BNCT, as shown in Figure 1B and C. The only adverse effect was hair loss in neutron-irradiation field, as shown in Figure 1C. MRI showed the further reduction of tumor and the disappearance of the cerebellar edema (Figure 2C and C'), 3 months after BNCT. Also F-BPA-PET taken 2 months after BNCT showed faint tracer uptake, indicating some metabolic change at least by this treatment (Figure 3A' and B', L/N ratio as 1.2).

Discussion

Radiation-induced osteosarcoma is not common. It has an aggressive nature, high recurrence rate, and poor prognosis. A standard therapy protocol has not yet been established for non-resectable tumors, but it was reported that particle radiotherapy (treatment with proton and carbon beams) had a therapeutic effect on these tumors [7,13].

In the present case, the tumor was chemo-resistant and difficult to totally resect because it invaded the left transverse and sigmoid venous sinuses. In addition, the subcutaneously extended tumor invaded the surface of the skin, and we thus suspected that a skin deficit due to surgery was inevitable and that particle radiotherapy for this tumor was likely to cause severe radiation-induced adverse effects on the scalp. The tumor was radiation-induced, and the cerebellum and overlying scalp had a history of X-ray treatment. Moreover, osteosarcomas have the characteristic of being radioresistant, i.e., X-ray-resistant. In light of these medical circumstances, we chose BNCT as the treatment modality for this patient. In the present case, the patient was successfully treated by BNCT without skin damage even though her tumor invaded the superficial scalp.

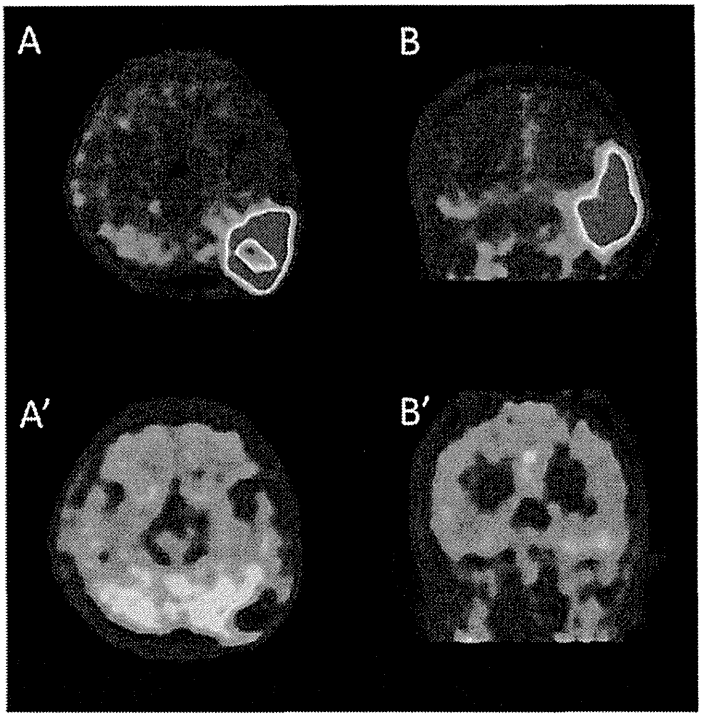

Figure 3 Fluoride-labeled boronophenylalanine-PET imaging of the brain before and after BNCT. Fluoride-labeled boronophenylalanine-PET imaging taken 1 month prior to BNCT (**A** and **B**) and 2 months after BNCT (**A′** and **B′**). **A** and **A′**: axial imaging, **B** and **B′**: coronal imaging. In **A** and **B**, L/N ratio was calculated as 5.0. This is theoretical proof of tumor selective destruction using BPA in BNCT. Also absorbed doses were simulated with this L/N ratio. 2 months after BNCT, **A′** and **B′** show the decreased L/N ratio as 1.2, indicating the marked effectiveness.

We recently reported the effectiveness of BNCT for radiation-refractory high-grade meningiomas [10]. In that report, we speculated that the difference in tumor shrinkage between the alpha and lithium particles provided by BNCT and other particles such as carbon and protons may be ascribed to the difference in LET noted above and their fraction size [10].

Other types of particle radiotherapy and some stereotactic radiotherapies which have been tried recently for tumors were applied as multi-fraction. The reduction of

Table 1 Estimated dose distribution at the central axis of neutron-irradiation field

Depth (cm)	Total dose (tumor) (Gy-eq)	Total dose (skin) (Gy-eq)	Total dose (mucosa) (Gy-eq)	Total dose (brain) (Gy-eq)	Thermal neutron (Gy-eq)	Fast neutron (Gy-eq)	γ-ray (Gy-eq)	Boron dose (tumor) (Gy-eq)
0.00	5.28E + 01	1.24E + 01	2.08E + 01	8.37E + 00	5.05E-01	2.13E + 00	1.00E + 00	4.92E + 01
0.50	6.79E + 01	----------	2.61E + 01	9.90E + 00	6.56E-01	1.87E + 00	1.22E + 00	6.41E + 01
1.00	8.06E + 01	----------	3.06E + 01	1.12E + 01	7.83E-01	1.64E + 00	1.43E + 00	7.67E + 01
1.50	8.47E + 01	----------	3.20E + 01	1.16E + 01	8.24E-01	1.35E + 00	1.63E + 00	8.09E + 01
2.00	9.00E + 01	----------	3.39E + 01	1.21E + 01	8.77E-01	1.17E + 00	1.80E + 00	8.62E + 01
2.50	9.38E + 01	----------	3.53E + 01	1.26E + 01	9.13E-01	1.11E + 00	1.92E + 00	8.98E + 01
3.00	9.55E + 01	----------	3.58E + 01	1.27E + 01	9.31E-01	9.77E-01	2.02E + 00	9.16E + 01
3.50	9.53E + 01	----------	3.57E + 01	1.27E + 01	9.30E-01	8.63E-01	2.09E + 00	9.14E + 01
4.00	9.18E + 01	----------	3.44E + 01	1.22E + 01	8.94E-01	7.72E-01	2.11E + 00	8.80E + 01
4.50	8.62E + 01	----------	3.24E + 01	1.16E + 01	8.38E-01	6.91E-01	2.10E + 00	8.26E + 01
5.00	7.97E + 01	----------	3.00E + 01	1.08E + 01	7.74E-01	6.18E-01	2.08E + 00	7.62E + 01
5.50	7.15E + 01	----------	2.70E + 01	9.79E + 00	6.93E-01	5.54E-01	1.99E + 00	6.82E + 01
5.80	6.77E + 01	----------	2.56E + 01	9.31E + 00	6.55E-01	5.12E-01	1.95E + 00	6.45E + 01

Table 2 RBE (relative biological effectiveness) factor

Radiation	Tumor	Brain	Skin
Thermal neuton	3.0	3.0	3.0
Epithermal neutron	3.0	3.0	3.0
^{10}B (n,α)^{7} Li: BPA	3.8	1.35	2.5
γ-ray dose	1.0	1.0	1.0

the tumor mass was thus not very prominent, and it was difficult to improve the patients' symptoms by means other than BNCT. BNCT can deliver high dose particles in a tumor-selective fashion in a single session, and in some cases the resulting reduction of the tumor was fast; this rapid shrinkage might contribute to the prompt elimination of symptoms [10]. Indeed, the present patient, within a very short time, exhibited improvement of her gait disturbance due to cerebellar ataxia.

Only a couple of articles were published with regard to pre-clinical study of BNCT for osteosarcoma in in vitro cell culture and animal experiments [14-17]. Among them, Russian research group reported successful treatment of dog osteosarcoma case by BNCT. Also only one preliminary report was published with regard to a BNCT-treated osteosarcoma case in head and neck region with limited description, so far [18]. We are not sure of the compound biological effectiveness (CBE) of BPA for osteosarcomas, and we were only able to estimate CBE as being the same for glioblastoma (i.e., 3.8) [19] as we did for high-grade meningioma [10]. For the estimation of the prescribed dose for this case, we adopted the reported value of CBE and relative biological effectiveness of neutron itself for tumors and normal tissues [20]. Thereafter the estimated tumor dose was uncertain in this case. However, as a result of the BNCT, the tumor shrank rapidly, the patient's clinical symptoms improved, metabolically scarce uptake of the amino-acid tracer was observed in the follow-up PET imaging and no serious damage was observed in the scalp and brain, so far at 6 months after BNCT, although the observation period was short.

Based on this outcome, we found that BNCT was an effective treatment for our patient. However, careful follow-up or the use of bevacizumab may be necessary in some cases [21], because WBRT that has been already performed may cause brain radiation necrosis.

We experienced only a case of successful treatment of BNCT for radiation-induced osteosacoma. Hopefully these potential therapeutic effects will be applicable for non-radiation-induced osteosarcomas which are generally refractory for other treatment modalities.

Conclusions

BNCT is an effective treatment for non-resectable radiation-induced skull osteosarcoma. We suggest that BNCT is the only effective therapy for tumors that have invaded the skin. Further applications of BNCT for similar cases are expected.

Competing interests

The authors declare that they have no competing interests.

Authors' contributions

S-IM conceived of the study and participated in the follow-up of the patient. GF, SK, NK, MS and KO applied BNCT in the atomic reactor. YS simulated BNCT dose. HS and TK participated in patient care in the hospital. MT and TT referred the patient for S-IM and also participated in the patient care and follow-up at the out-patient clinic. All authors read and approved the final manuscript.

Acknowledgement

We appreciate Dr. Silva Bortolussi, National Institute for Nuclear Physics (INFN) Section of Pavia, Italy for the critical reading of the manuscript and fruitful discussion.

Author details

[1]Department of Neurosurgery, Osaka Medical College, Takatsuki, Japan. [2]Particle Radiation Oncology Research Center, Kyoto University Research Reactor Institute, Kumatori, Japan. [3]Division of Radiation Life Science, Kyoto University Research Reactor Institute, Kumatori, Japan. [4]Division of Innovative Cancer Therapy, and Department of Surgical Neuro-Oncology The Institute of Medical Science, The University of Tokyo, Tokyo, Japan. [5]Cancer Center, Osaka Medical College, Takatsuki, Japan.

Received: 8 September 2014 Accepted: 14 October 2014
Published online: 04 November 2014

References

1. Patel AJ, Rao VY, Fox BD, Suki D, Wildrick DM, Sawaya R, DeMonte F: **Radiation-induced osteosarcomas of the calvarium and skull base.** *Cancer* 2011, 117:2120–2126.
2. Amendola BE, Amendola MA, McClatchey KD, Miller CH Jr: **Radiation-associated sarcoma: a review of 23 patients with postradiation sarcoma over a 50-year period.** *Am J Clin Oncol* 1989, 12:411–415.
3. Cahan WG, Woodard HQ, Higinbotham N, Stewart F, Coley B: **Sarcoma arising in irradiated bone; report of 11 cases.** *Cancer* 1948, 1:3–29.
4. Arlen M, Higinbotham NL, Huvos AG, Marcove RC, Miller T, Shah IC: **Radiation-induced sarcoma of bone.** *Cancer* 1971, 28:1087–1099.
5. Murray EM, Werner D, Greeff EA, Taylor DA: **Postradiation sarcomas: 20 cases and a literature review.** *Int J Radiat Oncol Biol Phys* 1999, 45:951–961.
6. Patel RD, Gadgil NM, Khare M, Majethia N: **Radiation-induced intracranial osteosarcoma: a case report.** *J Postgrad Med* 2014, 60:218–219.
7. Imai R, Kamada T, Tsuji H, Tsujii H, Tsuburai Y, Tatezaki S: **Cervical spine osteosarcoma treated with carbon-ion radiotherapy.** *Lancet Oncol* 2006, 7:1034–1035.
8. Mankin HJ, Hornicek FJ, Rosenberg AE, Harmon DC, Gebhardt MC: **Survival data for 648 patients with osteosarcoma treated at one institution.** *Clin Orthop Relat Res* 2004, 429:286–291.
9. Granados-Garcia M, Luna-Ortiz K, Castillo-Oliva HA, Villavicencio-Valencia V, Herrera-Gomez A, Mosqueda-Taylor A, Aguilar-Ponce JL, Poitevin-Chacon A: **Free osseous and soft tissue surgical margins as prognostic factors in mandibular osteosarcoma.** *Oral Oncol* 2006, 42:172–176.
10. Kawabata S, Hiramatsu R, Kuroiwa T, Ono K, Miyatake S: **Boron neutron capture therapy for recurrent high-grade meningiomas.** *J Neurosurg* 2013, 119:837–844.
11. Kawabata S, Yang W, Barth RF, Wu G, Huo T, Binns PJ, Riley KJ, Ongayi O, Gottumukkala V, Vicente MG: **Convection enhanced delivery of carboranylporphyrins for neutron capture therapy of brain tumors.** *J Neuro-Oncol* 2011, 103:175–185.
12. Miyashita M, Miyatake S, Imahori Y, Yokoyama K, Kawabata S, Kajimoto Y, Shibata MA, Otsuki Y, Kirihata M, Ono K, Kuroiwa T: **Evaluation of fluoride-labeled boronophenylalanine-PET imaging for the study of radiation effects in patients with glioblastomas.** *J Neuro-Oncol* 2008, 89:239–246.
13. Blattmann C, Oertel S, Schulz-Ertner D, Rieken S, Haufe S, Ewerbeck V, Unterberg A, Karapanagiotou-Schenkel I, Combs SE, Nikoghosyan A, Bischof M, Jakel O: **Non-randomized therapy trial to determine the safety and**

efficacy of heavy ion radiotherapy in patients with non-resectable osteosarcoma. *BMC Cancer* 2010, 10:96.
14. Bortolussi S, Ciani L, Postuma I, Protti N, Luca R, Bruschi P, Ferrari C, Cansolino L, Panza L, Ristori S, Altieri S: Boron concentration measurements by alpha spectrometry and quantitative neutron autoradiography in cells and tissues treated with different boronated formulations and administration protocols. *Appl Radiat Isot* 2014, 88:78–80.
15. Ferrari C, Zonta C, Cansolino L, Clerici AM, Gaspari A, Altieri S, Bortolussi S, Stella S, Bruschi P, Dionigi P, Zonta A: Selective uptake of p-boronophenylalanine by osteosarcoma cells for boron neutron capture therapy. *Appl Radiat Isot* 2009, 67:S341–S344.
16. Mitin VN, Kulakov VN, Khokhlov VF, Sheino LN, Bass LP, Kozolofskaya NG, Zaitsev KN, Potnov AA, Yagnikov SA, Shiraev SV: BNCT for Canine Osteosarcoma from Advances in Neutron Capture Therapy 2006. In *Proceedings of 12th International Congress on Neutron Capture Therapy. 9–13 October 2006.* Edited by Nakagawa Y. 2006:135–138.
17. Hsu CF, Lin SY, Peir JJ, Liao JW, Lin YC, Chou FI: Potential of usingboric acid as a boron drug for boron neutron capture therapy for osteosarcoma. *Appl Radiat Isot* 2011, 69:1782–1785.
18. Kato I, Ono K, Sakurai Y, Ohmae M, Maruhashi A, Imahori Y, Kirihata M, Nakazawa M, Yura Y: Effectiveness of BNCT for recurrent head and neck malignancies. *Appl Radiat Isot* 2004, 61:1069–1073.
19. Miyatake S, Kawabata S, Kajimoto Y, Aoki A, Yokoyama K, Yamada M, Kuroiwa T, Tsuji M, Imahori Y, Kirihata M, Sakurai Y, Masunaga S, Nagata K, Maruhashi A, Ono K: Modified boron neutron capture therapy for malignant gliomas performed using epithermal neutron and two boron compounds with different accumulation mechanisms: an efficacy study based on findings on neuroimages. *J Neurosurg* 2005, 103:1000–1009.
20. Coderre JA, Morris GM: The radiation biology of boron neutron capture therapy. *Radiat Res* 1999, 151:1–18.
21. Miyatake S, Kawabata S, Hiramatsu R, Furuse M, Kuroiwa T, Suzuki M: Boron neutron capture therapy with bevacizumab may prolong the survival of recurrent malignant glioma patients: four cases. *Radiat Oncol* 2014, 9:6.

doi:10.1186/s13014-014-0237-z
Cite this article as: Futamura *et al.*: A case of radiation-induced osteosarcoma treated effectively by boron neutron capture therapy. *Radiation Oncology* 2014 9:237.

OPEN ACCESS Freely available online

PLOS | ONE

Prognostic Factors for Survival in Patients with High-Grade Meningioma and Recurrence-Risk Stratification for Application of Radiotherapy

Shigeru Yamaguchi[1], Shunsuke Terasaka[1]*, Hiroyuki Kobayashi[1], Katsuyuki Asaoka[5], Hiroaki Motegi[1], Hiroshi Nishihara[2], Hiromi Kanno[2], Rikiya Onimaru[3], Yoichi M. Ito[4], Hiroki Shirato[3], Kiyohiro Houkin[1]

1 Department of Neurosurgery, Hokkaido University Graduate School of Medicine, Sapporo, Japan, **2** Department of Pathology, Hokkaido University Graduate School of Medicine, Sapporo, Japan, **3** Department of Radiation Oncology, Hokkaido University Graduate School of Medicine, Sapporo, Japan, **4** Department of Biostatistics, Hokkaido University Graduate School of Medicine, Sapporo, Japan, **5** Department of Neurosurgery, Teine-keijinkai Hospital, Sapporo, Japan

Abstract

Background: Radiotherapy for high-grade meningioma (HGM) is one of the essential treatment options for disease control. However, appropriate irradiation timing remains under debate. The object of this study is to discern which prognostic factors impact recurrence in HGM patients and to propose a risk-stratification system for the application of postoperative radiotherapy.

Methods: We retrospectively reviewed 55 adult patients who were diagnosed with Grade II and III intracranial meningioma. Cox regression models were applied to the analysis for impact on early recurrence in HGM patients without postoperative radiotherapy.

Results: Grade III malignancy ($P = 0.0073$) and transformed histology ($P = 0.047$) proved to be significantly poor prognostic factors of early recurrence by multivariate analysis. The other candidates for recurrence factors were Simpson Grade 3–5 resection, preoperative Karnofsky Performance status $<= 70\%$, and MIB-1 labeling index $>= 15\%$. According to these prognostic factors, postoperative HGM patients could be stratified into three recurrence-risk groups. The prognoses were significantly different between each group, as the 3-year actual recurrence-free rates were 90% in low-risk group, 31% in intermediate-risk group, and 15% in high-risk group.

Conclusion: We propose recurrence-risk stratification for postoperative HGM patients using clinically available factors. Our results suggest that the prognosis for patients with high-risk HGMs is dismal, whereas HGM patients belonging to the low-risk group could have favorable prognoses. This stratification provides us with the criteria necessary to determine whether to apply adjuvant radiotherapy to postoperative HGM patients, and to also help identify potentially curable HGMs without adjuvant radiotherapy.

Citation: Yamaguchi S, Terasaka S, Kobayashi H, Asaoka K, Motegi H, et al. (2014) Prognostic Factors for Survival in Patients with High-Grade Meningioma and Recurrence-Risk Stratification for Application of Radiotherapy. PLoS ONE 9(5): e97108. doi:10.1371/journal.pone.0097108

Editor: James Bradley Elder, The Ohio State University Medical Center, United States of America

Received February 17, 2014; **Accepted** April 15, 2014; **Published** May 12, 2014

Funding: The authors have no support or funding to report.

Competing Interests: The authors have declared that no competing interests exist.

* E-mail: terasas@med.hokudai.ac.jp

Introduction

Although meningiomas have become the most common primary brain tumor and the majority of these are considered histologically benign [1], there is low incidence of high-grade meningiomas (HGMs), defined as Grade II and Grade III by WHO classification, and their biological behaviors are occasionally unpredictable [2,3]. In particular, the aggressive nature of HGMs in the event of tumor relapse has been noted, and recurrent HGMs are generally difficult to manage.

Retrospective studies have demonstrated that adjuvant radiotherapy can contribute to a favorable prognosis for patients with HGM [2,4]. However, the optimal timing of radiotherapy remains unclear for many clinicians. Some studies recommend that patients for whom gross total resection of the HGM cannot be achieved should receive postoperative radiotherapy [5,6], whereas other reports recommend that all patients with HGMs should receive postoperative irradiation regardless of the extent of the resection [2,4]. Thus, the indication of postoperative radiotherapy for HGMs is only discussed with respect to the extent of resection. However, is the extent of resection a sufficient clinical prognostic factor, especially by itself, when we make a decision regarding irradiation timing for postoperative HGM patients?

To elucidate the influence of radiotherapy on treatment outcomes and to discuss suitable irradiation timing in patients with HGMs, we rigorously reviewed the clinical factors and outcomes of HGM patients treated at our institutions and paid special consideration to radiation timing. We performed multivariate analysis of clinical and pathological factors, which are typically available in the postoperative period, leading to the

identification of possible prognostic factors for the risk of recurrence for HGM patients without postoperative radiotherapy. Based on the results of this analysis, we propose a stratification of recurrence-risk. In addition, an important aim of this study was to identify the patient group that did not require postoperative radiotherapy using appropriate criteria.

Materials and Methods

Patients

This study was approved by the Internal Review Board on Ethical Issues of Hokkaido University Hospital and appropriate written informed consents were obtained from eligible patients. A retrospective review was performed at the Hokkaido University Hospital and our affiliated institutions on patients since 1995 that were over 20 years old with a histological diagnosis of HGM, including WHO Grade II (n = 42) and Grade III (n = 13). We referred to pathological reports to identify HGM patients, and their diagnoses were re-confirmed by senior neuropathologists (H.N. and H.K.) according to WHO 2007 criteria, as described below. Pediatric patients, spinal meningiomas, and radiation-induced meningiomas were excluded in this study.

Ultimately, there were 27 males and 28 females with a mean age of 60±15 years (range: 23–84). Regarding histological classification, Grade II meningiomas included two clear cell meningiomas and one chordoid meningioma, and Grade III meningiomas included one papillary meningioma and one rhabdoid meningioma on which we have reported previously [7]. In this study, we included patients with HGMs that were transformed from benign (Grade I) meningiomas at first presentation. Those tumors are defined as "transformed", whereas the tumors that were diagnosed as HGM at first presentation were defined as "de novo" [8]. Ten Grade II tumors were categorized as transformed HGM; the mean interval between benign and Grade II histology was 10±9 years (range: 1–30 years). There are no cases that had progressed directly from benign to Grade III included in this series. All patients' characteristics are shown in Table 1.

Clinical Parameters and Outcome Assessment

Tumor size was defined by the largest diameter of contrast enhancement on the preoperative imaging. Each patient's preoperative condition was assessed by the Karnofsky performance status (KPS). Tumor locations were categorized into five groups: convexity, found in 17 cases; parasagittal/falcine/tentorial, in 20 cases; sphenoid ridge, in 9 cases; skull base, in 5 cases; and other, in 4 cases including intraventricular (n = 2), orbital (n = 1), and interosseous (n = 1). The endpoints were recurrence-free survival (RFS) and overall survival (OS), which were measured from the time of first HGM diagnosis. In the patients with transformed HGM, their time interval from benign to high-grade was not included in the survival analysis. All patients were followed in our institutions until death or their last visit. The time of recurrence was defined as the development of either clinically and radiographically evident relapse, or tumor re-growth. Patients without event were regarded as censored observations at the last follow-up visit.

Treatment

Simpson Grades 1 and 2 resections were designated as gross total resection confirmed by both operation record and postoperative radiographic appearance [9]. Postoperative adjuvant radiotherapy was administered to 19 patients, while the remaining 36 patients had irradiation deferred in case of relapse or tumor re-growth. The patients with postoperative radiotherapy were classified into the "early" irradiation group, and the others were classified into the "deferred" irradiation group. Postoperative radiotherapy was administered at the discretion of the physician. At the time of this analysis, 15 out of 36 patients in the deferred irradiation group had received irradiation for recurrent tumors. In terms of radiotherapy, patients were treated with X-ray based radiotherapy. The range of cumulative irradiation dose were from 50 Gy to 60 Gy using 2.0 Gy as the daily dose. Patients with HGM who were treated by other radiotherapies, such as gamma-knife or Boron Neutron Capture therapy (BNCT), are not included in this series.

Pathological Examination

All patients were re-evaluated to confirm the pathological diagnosis according to WHO 2007 criteria by senior neuropathologists. They counted mitoses per 10 high-power fields (HPFs, ×400) and the 5 prognostic histological parameters of hypercellularity, macronucleoli, small cell formation, patternless architecture and necrosis as 0 (no) or 1 (yes). The sum of each parameter was designated as an atypical score. Cases with 4 or more mitoses per 10 HPFs or with an atypical score greater or equal to 3 correspond to atypical meningioma. Cases with an obviously malignant cytology resembling that of carcinoma, melanoma, high-grade sarcoma, or a markedly elevated mitotic index (20 or more mitoses per 10 HPFs) correspond to anaplastic meningioma [10]. Cellular proliferation was assessed using the MIB-1 labeling index by immunohistochemistry. The quantification of the MIB-1 labeling index was performed by H.K., who was blinded to the clinical information. Eventually, MIB-1 labeling was made available to index of 50 out of 55 cases.

Statistical Analysis

All statistical analyses were carried out in R statistical environment version 3.0.2. Continuous variable data were expressed with standard deviation (SD). The mean of continuous variables was compared by Welch two sample t-tests, the median of continuous variables was compared by Mann-Whitney U test or Kruskal-Wallis test, and the distribution of categorical variables was compared by Pearson's Chi-squared test or Fisher's exact test according to the counts of expected frequencies. Estimated survival curves were shown by Kaplan-Meier method, and a log-rank test was used for the comparison.

To analyze prognostic factors for the risk of recurrence in the deferred irradiation group, the patient and the treatment characteristics were evaluated for association with the time to recurrence using Cox proportional hazards regression model. The analyzed characteristics included the patient's age, gender, preoperative KPS, previous diagnosis of meningioma, location of the tumor, extent of resection, MIB-1 labeling index, and the histological grade. A hazard ratio, with 95% confidence intervals (CIs) from a Cox model, summarized the effect; a non-parametric CI was calculated by the Greenwood formula. In multivariate analysis, the factors for which the *P*-value was below 0.1 in univariate analysis were selected. The factor of the MIB-1 labeling index could not be applied in multivariate analysis due to significant correlation with the histological grade ($P = 0.015$, Fig. 1). Statistical significance was given to p-values <0.05.

Results

Patient characteristics

Table 1 shows the patient characteristics between the early irradiation group and the deferred irradiation group. In comparison to the deferred irradiation group, the number of Grade III

Table 1. Descriptive statistics of study samples by postoperative radiotherapy.

	All patients (n = 55)	Early RT group (n = 19)	Deferred RT group (n = 36)	P-value[a]
Age (year), mean ± SD	60±15	58±15	62±16	0.38[b]
Gender				0.13[c]
Male	27	12	15	
Female	28	7	21	
Preoperative KPS (%)				0.59[c]
80–100%	35	13	22	
<80%	20	6	14	
Location				0.46[d]
Convexity	17	4	13	
Parasagittal/Falcial/Tentorial	20	8	12	
Sphenoid ridge	9	2	7	
Skull Base	5	3	2	
Others	4	2	2	
Tumor size (cm), mean ± SD	5.4±1.8	5.4±1.9	5.3±1.8	0.91[b]
Benign meningioma at first presentation				0.74[c]
No (de novo)	45	16	29	
Yes (transformed)	10	3	7	
Extent of Resection (Simpson Grade)				0.23[d]
Grade 1	14	4	10	
Grade 2	12	2	10	
Grade 3–5	29	13	16	
Histology				0.10[d]
Grade II	42	12	30	
Grade III	13	7	6	
MIB-1 labeling index (%), mean ± SD	11.2±7.4	12.6±7.2	10.4±7.5	0.30[b]
Median follow-up period (months)	43.9	50.1	40.3	0.62[e]
Endpoint				
Recurrence (%)	34 (62%)	11 (58%)	23 (94%)	
Death (%)	17 (31%)	9 (47%)	8 (22%)	

Abbreviations: SD, standard deviation; RT, radiotherapy.
[a]Comparison between early irradiation group and deferred irradiation group.
P-values were calculated by [b]Welch t-test, [c]Pearson's Chi-squared test, [d]Fisher's exact test and [e]Mann-Whiteny.
U-test.
doi:10.1371/journal.pone.0097108.t001

meningioma patients is higher in the early irradiation group, but the difference is not statistically significant (P = 0.10). There were no significant differences with respect to other clinical factors, nor to the extent of the resection. 34 out of the 55 tumors were found to have recurred and 17 patients died as a result of tumor progression. The median follow-up period of all patients was 43.9 months (range: 3.1–182.9 months), and there was no significant difference in median follow-up period between the two groups (P = 0.62). 21 out of 36 patients in the deferred irradiation group did not require irradiation at the time of this analysis. The median follow-up period of these 21 patients was 36.4 months.

Prognostic factors in deferred irradiation group

To identify which clinical factors influenced the recurrence of HGMs, we analyzed the deferred irradiation group using the Cox model (n = 36, Table 2). According to multivariate analysis, two parameters were found to be significant poor prognostic factors of early recurrence: Grade III malignancy (P = 0.0073) and transformed histology (P = 0.047). Although Simpson Grade 3–5 resection was one of the candidates of poor prognostic factors in univariate analysis (P = 0.0034), the extent of resection was not found to influence tumor recurrence in multivariate analysis (P = 0.82). The other possible poor prognostic factor was poor preoperative KPS (P = 0.019, in univariate analysis). Although we could not apply the MIB-1 labeling index of the tumor in multivariate analysis, univariate analysis indicated that a high MIB-1 labeling index, defined as more than 15%, might be a possible candidate for a prognostic factor for early recurrence (P = 0.020).

Recurrence-risk stratification

Based on the analyzed results of the Cox model, we propose to stratify the recurrence-risk group according to these prognostic factors (Table 3). For the high-risk group, two classifiers are selected that were identified as significant poor prognostic factors by multivariate analysis: Grade III malignancy, and transformed histology. For the intermediate-risk group, three prognostic factors are selected as classifiers based on univariate analysis as follows:

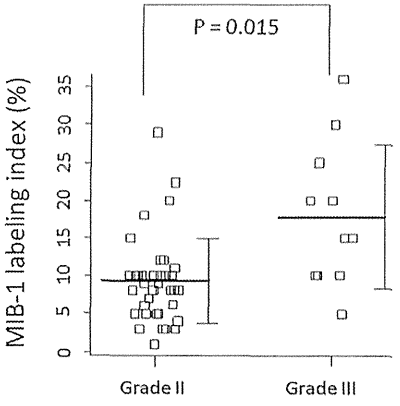

Figure 1. The MIB-1 labeling index of Grade II and Grade III meningioma. The mean MIB-1 labeling index of Grade II and Grade III meningioma are 9.3% and 17.8%, respectively, and these mean value are significantly different ($p = 0.015$). The bars represent the mean values and standard deviations.
doi:10.1371/journal.pone.0097108.g001

the patients with poor preoperative KPS, tumors with Simpson grade 3–5 resection, and high proliferative tumors suggested by high MIB-1 labeling index (more than 15%). The tumors that meet any of the above criteria are stratified into each recurrence-risk group, and the patients whose clinical and pathological characteristics do not match the above criteria are stratified into a low-risk group.

Figure 2 shows Kaplan-Meier curves of the patients in the deferred irradiation group according to the recurrence-risk stratification we propose. The prognosis shows a significant difference not only in RFS but also in OS among the recurrence-risk stratified groups ($p<0.001$ in PFS, $P = 0.001$ in OS). The 3-year actual recurrence-free rates of the low-risk, intermediate-risk, and high-risk groups were 90%, 31%, and 15%, respectively. In the intermediate-risk group, the median RFS is 28.4 months. Although the RFS of the intermediate-risk group was poor compared to the low-risk group, all patients who were stratified in intermediate-risk and low-risk group have been alive through follow-up periods. Finally, the prognosis of the high-risk group was dismal. The median RFS and OS of the high-risk group are 11.2 months and 52.1 months, respectively.

In addition, when the patients who received early irradiation had been assigned to this recurrence-risk stratification, 10 out of 19 tumors fell into the high-risk group, and 9 out of 19 tumors were in the intermediate-risk group. Figure 3 shows the RFS in the high-risk group and intermediate-risk group according to the postoperative radiation. As clearly shown, the prognosis of the patients with high-risk HGMs who were treated by early irradiation was significantly better ($P = 0.019$), whereas there were no significant prognostic differences between early irradiation and deferred irradiation in the intermediate-risk HGMs ($P = 0.34$).

Discussion

Since radical resection of meningioma is widely agreed to cause an improvement of prognosis [11], neurosurgeons always attempt to resect the tumor at the highest possible extent irrespective of histological subtype or tumor location. Although some promising antineoplastic agents, such as trabectedin [12] or histone deacetylase inhibitors [13], are being used in preclinical studies, commonly acceptable chemotherapies for HGMs are currently

Table 2. Cox regression Hazard model on RECURRENCE FREE SURVIVAL in deferred irradiation group.

		Univariate analysis			Multivariate analysis		
Factors		Hazard ratio	95% CI	P-value	Factors	Hazard ratio	95% CI
Age*		1.017	0.988–1.05	0.26			
Gende	Male	0.784	0.333–1.84	0.58			
Location	Not convexity	1.852	0.679–5.05	0.229			
Preoperative KPS (%)	80–100%	0.360	0.153–0.844	0.019	0.421	0.166–1.07	0.069
Tumor size	>6.0 cm	1.551	0.632–3.81	0.338			
Histology	Grade III	4.648	1.74–12.4	0.0022	6.68	1.67–26.8	0.0073
Histology at presentation	transformed	3.16	1.26–7.95	0.0144	4.33	1.02–18.4	0.047
Extent of resection (Simpson grade)	Grade 3–5	3.95	1.58–9.89	0.0034	1.167	0.317–4.30	0.82
MIB-1 labeling index (%) (n = 35)	10–15%	0.975	0.323–2.95	0.96	NA	NA	NA
	>15%	3.683	1.23–11.0	0.020	NA	NA	NA

Abbreviations: CI, confidence interval; KPS, Karnofsky performance status; NA, no assessment.
*continuous variable.
doi:10.1371/journal.pone.0097108.t002

Table 3. Recurrence-risk stratification of high-grade meningioma.

Risk group	Classifiers
High-risk group	1 Grade III malignancy
	2 Transformed histology
Intermediate-risk group	1 Poor preoperative KPS score (less than 70%)
	2 Simpson grade 3–5 resection
	3 High MIB-1 labeling index (more than 15%)
Low-risk group	None of matched above factors

Abbreviation: KPS, Karnofsky performance status.
doi:10.1371/journal.pone.0097108.t003

unavailable. Therefore, radiotherapy remains the sole treatment option after surgical resection of HGMs, and the timing of radiotherapy is of great concern to physicians and has been discussed in several retrospective analyses [2,4,5,6].

There is no doubt that radiotherapy for HGMs is beneficial for controlling tumor recurrence and has demonstrated improvement in patient prognosis [2,4]. However, compared to other malignant brain tumors such as high-grade gliomas and medulloblastomas, the role of radiotherapy for HGMs remains ambiguous. Previously, some studies suggested that patients with atypical meningiomas for whom gross total resection is possible do not necessarily need postoperative radiotherapy [5,6]. In addition, Pearson et al. pointed out that the incidence of atypical meningiomas increased dramatically after 2004 due to the reclassification of WHO criteria [6]. Our series also show this trend, as 39 (71%) out of the 55 cases were diagnosed as HGMs after 2004. This fact might indicate that recent cases diagnosed as HGM might include cases that did not meet the old criteria, suggesting in turn that the number of surgically curable HGMs may have recently increased.

The main aim of this study is to attempt to identify the prognostic risk factors of early recurrence that are available at the time physicians decide whether postoperative irradiation should be performed. To eliminate the influence of radiotherapy, we specifically focused on HGM patients who did not received postoperative radiotherapy at primary HGM diagnosis. Thereafter, we stratified our patient pool into three recurrence-risk groups according to these factors, which were identified by multivariate and univariate analyses, and we validated the survival effect for each of these groups. Although this novel approach is debatable, we propose that it can provide some clues for the treatment strategy of this rare disease.

Through this analysis, we were able to identify two significant risk factors: Grade III malignancy and transformed histology. In terms of Grade III meningioma, previous reports evidently recommended postoperative radiotherapy regardless of the extent of resection [14,15]. Durand et al. evaluated the prognostic factors for high-grade meningioma on 199 adult patients. Although no significant difference was found in overall survival rate between the patients who had and had not received radiation adjuvant treatment, it was found that only the prognosis of Grade III meningioma could be improved by postoperative radiotherapy [16]. These results are consistent with our analysis.

The other significant poor risk factor is transformed malignancy. In our series, all transformed HGM cases ranged from benign to atypical. Nevertheless, the prognosis of these patients was significantly poor, as was that of the Grade III meningioma patients. With respect to glioblastoma, secondary malignancy is representative of a good prognostic factor [17], whereas the malignant transformation exhibited contrasting findings for HGM. This poor prognostic factor was also recognized by two previous

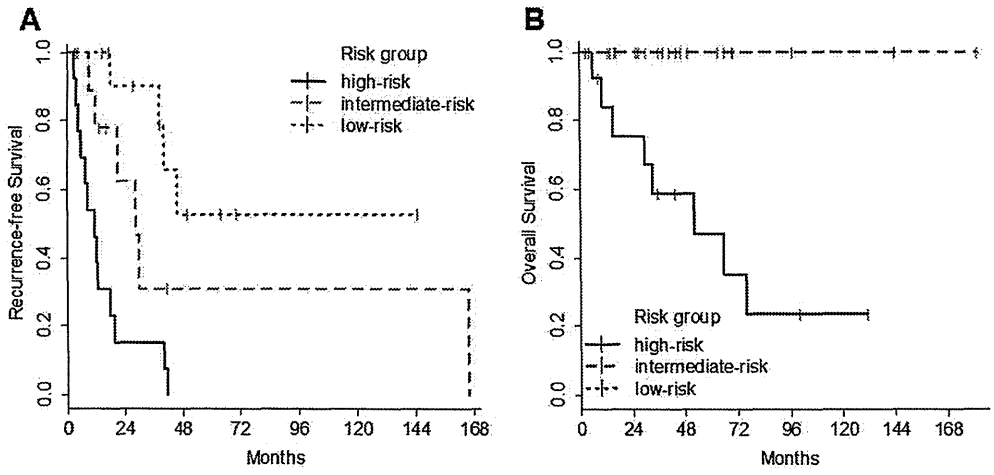

Figure 2. Kaplan-Meier estimates based on the recurrence-risk stratification. The graphs show recurrence-free survival (A) and overall survival (B) according to the recurrence-risk stratification defined as prognostic factors. Prognosis shows a significant difference in both RFS and OS among the recurrence-risk stratified groups ($p<0.001$ in PFS, $P=0.001$ in OS).
doi:10.1371/journal.pone.0097108.g002

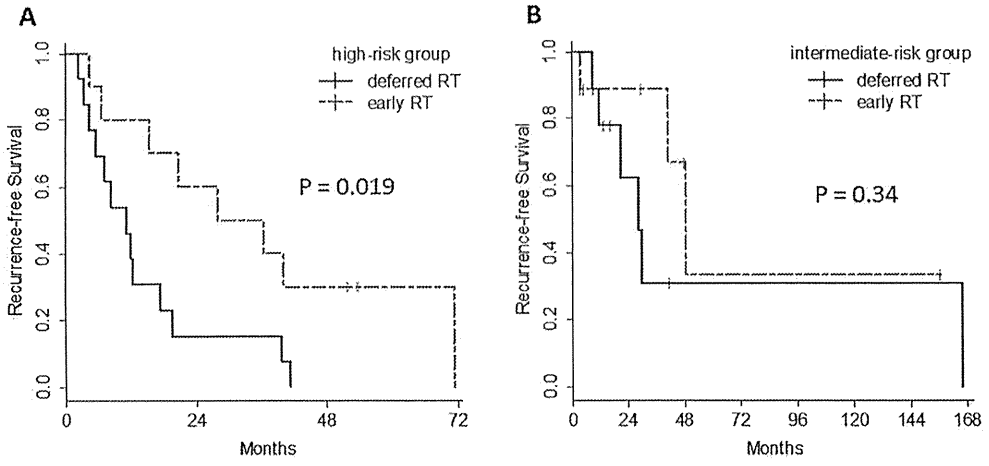

Figure 3. Recurrence-free survival analysis according to postoperative irradiation. Kaplan-Meier estimates of recurrence-free survival are illustrated according to the treatment option of postoperative irradiation in high-risk group (A) and intermediate-risk group (B). In high-risk group, the prognosis of the patients with early irradiation was significantly better (P = 0.019), whereas there were no significant prognostic differences between early irradiation and deferred irradiation in the intermediate-risk HGMs (P = 0.34). RT stands for radiation therapy.
doi:10.1371/journal.pone.0097108.g003

studies [8,18]. Interestingly, Krayenbühl et al. demonstrated the significant differences of histological characters, in addition to cytogenetic findings between "de novo" subgroup and "transformed" subgroup. They hypothesized that the "transformed" HGMs could comprise distinct subgroups of aggressive meningiomas compared to "de novo" HGMs [8]. In addition, Yang et al. reported that tumors with malignant transformation had a higher percentage of p53 overexpression than "de novo" tumors [18]. Their findings are consistent with our results, and can provide the biological clues toward a better understanding of the poor prognosis of this subpopulation.

For the classifiers of the intermediate-risk group, three risk factors were designated based on univariate analyses: patients' poor preoperative KPS, incomplete tumor resection, and tumors with high MIB-1 labeling indices. Our series failed to demonstrate a significant beneficial effect from gross total resection in multivariate analysis, suggesting that the extent of resection is not always a definitive prognostic factor for HGM patients. In addition, we adopted the MIB-1 labeling index as a prognostic factor by histological aspect. It is well known that the MIB-1 labeling index is routinely performed worldwide and recognized as one of the most reliable markers of proliferative tumor activity [19]. Compared to Grade III meningioma, it is commonly recognized that the diagnosis criteria of Grade II meningiomas are highly controversial despite the objective criteria of WHO classification. In actuality, the difference of mean MIB-1 labeling index among the studies was significant, ranging from 3.2%[18] to 15.81% [20]. To complement this interinstitutional or interobserver difference, the "high MIB-1 labeling index" became a proper objective factor to identify the tumors that might pose a potential risk for early recurrence.

For the treatment of high-risk HGM patients, we advocate postoperative radiotherapy regardless of the extent of resection. As shown in Figure 3A, early irradiation could contribute to prolonged recurrence-free survival of the patients with high-risk HGM. On the other hand, patients with low-risk HGMs should not be given up-front radiotherapy. Low-risk HGMs might be curable without irradiation and the patients may ultimately remain free of recurrent disease, as with the patients who undergo complete resection of benign meningiomas. In addition, in the instance that low-risk HGMs relapse, our data suggests that the recurrent tumor could be regulated via salvage operation or radiotherapy. Compared to the high-risk and low-risk groups, the biological behaviors and clinical courses of the intermediate-risk HGMs are heterogeneous. It is ambiguous whether the patients in the intermediate-risk group should receive postoperative radiotherapy. The Kaplan-Meier curves in Fig. 3B provide a visual representation of the recurrence pattern. These curves indicate that the intermediate-risk group included tumors with a high possibility of early recurrence, especially for the first three years following diagnosis, as well as tumors that are potentially curable without irradiation.

Conclusions

Although the influence of irradiation will likely be difficult to fully elucidate in a single-institution series, our scrupulous analysis provides a clue as to how to manage treatment for HGM patients. We propose recurrence-risk stratification using available clinical and histopathological factors for the purpose of making decisions regarding radiotherapy for postoperative HGM patients. Multicenter reviews and prospective studies are necessary to evaluate this stratification system for validity.

Author Contributions

Conceived and designed the experiments: SY ST KH HS. Performed the experiments: HN H. Kanno. Analyzed the data: SY YI. Contributed reagents/materials/analysis tools: ST H. Kobayashi KA HM RO. Wrote the paper: SY ST.

References

1. Claus EB, Bondy ML, Schildkraut JM, Wiemels JL, Wrensch M, et al. (2005) Epidemiology of intracranial meningioma. Neurosurgery 57: 1088–1095.

2. Adeberg S, Hartmann C, Welzel T, Rieken S, Habermehl D, et al. (2012) Long-term outcome after radiotherapy in patients with atypical and malignant